Received: 27 December 2022 | Revised: 8 July 2023 | Accepted: 12 July 2023

DOI: 10.1111/bre.12808

Basin Research | IAS EAGE | WILEY

RESEARCH ARTICLE

New detrital petrographic and thermochronologic constraints on the Late Cretaceous–Neogene erosional history of the equatorial margin of Brazil: Implications for the surface evolution of a complex rift margin

Maria Giuditta Fellin[1] | **Massimiliano Zattin**[2] | **Gian Gaspare Zuffa**[3] | **L. Fernando De Ros**[4] | **José A. Cupertino**[5] | **Rogério Schiffer De Souza**[6] | **J. Marinho Morais Neto**[7] | **Claudio Dalmonte**[8]

[1]Department of Earth Sciences, ETH Zurich, Zurich, Switzerland

[2]Department of Geosciences, University of Padova, Padua, Italy

[3]University of Bologna, Professor Alma Mater Studiorum, Bologna, Italy

[4]Geosciences Institute, Rio Grande do Sul Federal University, Porto Alegre – RS, Brazil

[5]Pontifical Catholic University of Rio Grande do Sul, Porto Alegre – RS, Brazil

[6]Pontifical Catholic University of Rio de Janeiro, Rio de Janeiro – RJ, Brazil

[7]PETROBRAS/EXP/PEN/AB-Exploration, Rio de Janeiro, Brazil

[8]University of Bologna, ATES Distretto Filippo Re, Bologna, Italy

Correspondence
Maria Giuditta Fellin, Department of Earth Sciences, ETH Zurich, Zurich, Switzerland.
Email: fellin@erdw.ethz.ch

Abstract

The equatorial margin of Brazil is an example of a rift margin with a complex landscape, dominated by an escarpment perpendicular to the continental margin, which testifies to an equally complex rift and post-rift surface and tectonic evolution. This has been the focus of a long debate on the driving mechanism for post-rift tectonics and on the amount of exhumation. This study contributes to this debate with new petrographic and thermochronologic data on 152 samples from three basins, Pará-Maranhão, Barreirinhas and Ceará, on the offshore continental platform. Our detrital record goes back to the rift time at ca. 100 Ma ago and outlines three major evolutionary phases of a changing landscape: a rift phase, with the erosion of a moderate rift escarpment, a Late Cretaceous-Palaeogene post-rift phase of major drainage reorganization and significant vertical erosion and a Late Oligocene-to-Recent post-rift phase of moderate vertical erosion and river headwater migration. We estimate that along the equatorial margin of Brazil, over a large onshore area, exhumation since the Late Cretaceous has totalled locally up to 2–2.5 km and since the late Oligocene did not exceed 1 km.

1 | INTRODUCTION

Divergent margins extend for thousands of kilometres along the rims of major continents. Yet, their surface evolution and their contribution to the bulk production of siliciclastic detritus and its weathering is often poorly constrained due to basic challenges in determining erosion rates of slowly eroding landscapes and their spatial and temporal changes at different time scales. Typical markers of the surface evolution along and near rift margins are peneplain surfaces that can only be dated if they are capped by fossiliferous sediments (e.g. Campbell et al., 2006), rare in continental deposits, or by datable weathering profiles, for instance, those containing U-rich, *in situ* growing minerals

as goethite (e.g. Vasconcelos et al., 2019). Alternatively, constraints on the surface evolution are commonly based on low-temperature thermochronology that measures the times and rates at which rocks approach the surface, and on cosmogenic nuclide dating that measures the time of exposure of rocks to cosmic rays (e.g. Belton et al., 2004; Wittman et al., 2011). However, these methods provide no direct measurements of how the surface topography varies through time and space but only indirect inferences that need testing against various constraints based on the combination and integration of multiple approaches.

This study contributes with new constraints on the erosional history of the equatorial margin of Brazil. This is a cratonic area that exposes crystalline basement and siliciclastic sedimentary rocks and that underwent a complex, still debated, Late Cretaceous and Cenozoic surface evolution (Garcia et al., 2019; Japsen et al., 2012; Morais Neto et al., 2005–2006, 2008, 2009, 2010, 2012; Morais Neto & Vasconcelos, 2010; Peulvast & Bétard, 2021; Sacek et al., 2019). The Atlantic margin of Brazil evolved since rifting between the African and South American plates in the Late Jurassic–Early Cretaceous. While along the eastern Brazilian margin the escarpment runs approximately along the coastline, along the SE-NW equatorial Brazilian margin, an escarpment, almost 1 km high, perpendicular to the margin (i.e. Serra de Ibiapaba; Figure 1), dominates a complex landscape. In addition to an unusual landscape, the equatorial Brazilian margin features an onshore stratigraphic record of post-rift phases of uplift and erosion alternating with phases of subsidence and deposition (Morais Neto et al., 2009). Our new petrographic and thermochronologic data on 152 samples from the offshore Pará-Maranhão, Barreirinhas and Ceará Basins provide information on the provenance of the clastic material and on its near-surface cooling record. This information permits reconstructing the evolution of the drainage routing system and to estimate the amount of exhumation in the onshore margin segment. Our findings indicate: (i) moderate erosion of the rift flank until the transition between Early and Late Cretaceous; (ii) a major drainage reorganization and erosional event during the Late Cretaceous; and (iii) little vertical erosion associated with headwater migration of river drainages from the late Oligocene to the present. Altogether, the arkosic composition, the pristine heavy mineral assemblage and the detrital thermochronologic age populations of the offshore sediments from the equatorial Brazilian margin testify to the progressive exhumation and exposure over larger areas of metasedimentary rocks. These rocks may have contributed significantly to the global production of siliciclastic detritus since the early Late Cretaceous.

Highlights

- Early Cretaceous-to-recent sandstones from the equatorial Brazilian margin are characterized by a dominantly arkosic composition and a pristine heavy mineral assemblage.
- The detrital signature changed during the Late Cretaceous likely in response to a major drainge reorganization and erosion in the source area.

2 | GEOLOGICAL BACKGROUND

Eastern equatorial Brazil comprises the Precambrian basement rocks of the Borborema Province, the Silurian-to-Triassic sedimentary rocks of the Parnaíba Basin and the Cretaceous-to-Cenozoic sedimentary covers that were deposited as and after South America and Africa rifted apart (Figure 1).

The Borborema Province is an assemblage of crustal blocks with Archean and Proterozoic gneissic–migmatitic rocks that were metamorphosed and intruded during the Brasiliano orogeny at ca. 750–500 Ma (e.g. Arthaud et al., 2008, 2015; Nascimento et al., 2015). One of these crustal blocks exposes a metamorphic complex (Ceará Complex) with Ediacaran high-grade metamorphism, up to eclogite facies preserved in aluminous metasedimentary rocks (Arthaud et al., 2015; Motta Garcia et al., 2014).

The Parnaíba Basin is a cratonic sag developed over Precambrian rocks (Cordani et al., 2009; Watts et al., 2018). The Silurian–Triassic sequence of this basin consists of siliciclastic sediments, showing repetitive transgressive-to-regressive cycles (Góes & Feijó, 1994). This sequence is overlain by Jurassic mafic volcanic rocks and, in the

FIGURE 1 Top: Relief model of the Brazilian Equatorial margin and north-eastern Brazil extracted from ETOPO1. Inset shows the location of the study area relative to Brazil. The Serra de Ibiapaba is a ca. 400-km-long cuesta, with an N-S trend perpendicular to the rift margin, which reaches 952 m of elevation and separates the Parnaíba Basin to the east from the Borborema Province to the west. C: Location of a breach into the Serra de Ibiapaba caused by a river that drains the lowlands to the east of the Serra de Ibiapaba towards the Parnaíba Basin. PM: Pereiro Massif, an elevated area capped by Miocene laterite (Gurgel et al., 2013). Bottom: Simplified geologic map of north-eastern Brazil with the location of the wells, from which samples were derived, and of the apatite fission-track ages on the basement rocks of the Brazilian equatorial margin (data from Harman et al., 1998; Cavalcante, 2006; Nóbrega et al., 2005; Morais Neto et al., 2008, 2009; Turner et al., 2008; Mojzeszowicz, 2009).

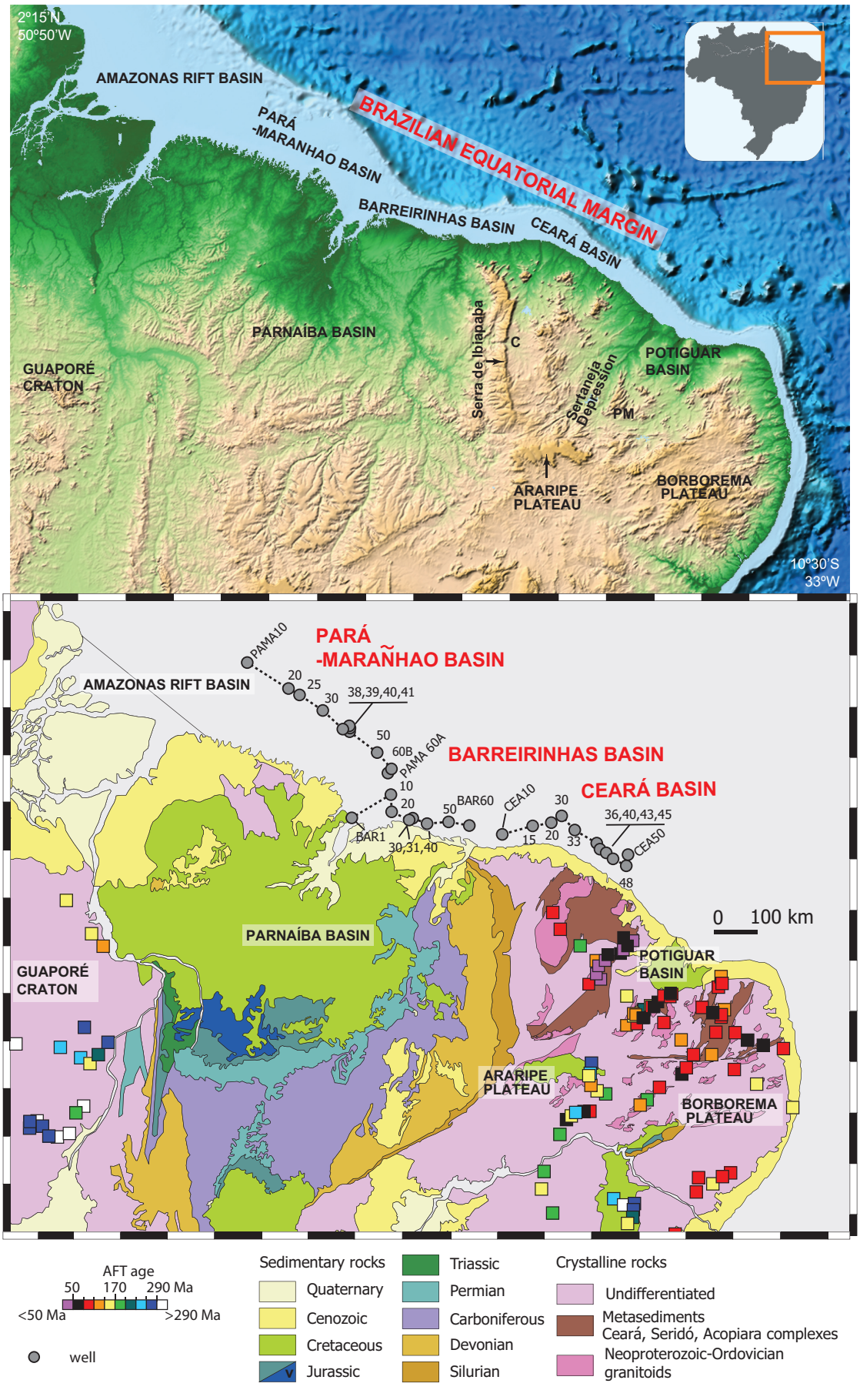

north-eastern portion of the Parnaíba basin, by Cretaceous shallow marine-to-transitional sediments.

The Equatorial Atlantic Rifting occurred during the Late Jurassic to the Early Cretaceous, along reactivated shear zones inherited from the Precambrian crust (Matos, 1992) and resulted in variable distribution and progression of extension (e.g. Heine et al., 2013). In the study area, several offshore and marginal basins, such as the Pará-Maranhão, Ceará and Barreirinhas Basins, record the transgression associated with rifting during the Aptian to lower Albian. During the Cretaceous until at least the early Palaeocene, the onshore part of the eastern continental margin remained largely a non-depositional site subjected to aerial exposure and the development of lateritic soil (Rossetti et al., 2013). During the Palaeocene–Oligocene (64–25 Ma; Morais Neto et al., 2008) and during the Miocene (22 and 17 Ma; Lima, 2008; Rossetti et al., 2013), two main depositional episodes occurred onshore. These are testified by Palaeocene–Oligocene continental deposits, which are preserved as remnant covers of several mesas in the Borborema Plateau area at altitudes from 500 to 760 m (e.g. Araripe Plateau; Figure 1), and by Miocene coastal siliciclastic formations preserved in cuestas along more than 4000 km of the littoral zone of the equatorial Brazilian margin (Rossetti et al., 2013; Figure 1). These deposits indicate that on the equatorial margin of Brazil, phases of non-deposition and erosion alternated with phases of subsidence and deposition (Garcia et al., 2019; Japsen et al., 2012; Morais Neto et al., 2008, 2009; Peulvast & Bétard, 2021; Rossetti et al., 2013; Sacek et al., 2019).

The long period since rifting features significant contractional deformation that is recorded both by the stratigraphic record and topography of the onshore continental margin and of the offshore basins. For instance, the offshore Ceará Basin records Late Cretaceous tectonic inversion related to the activity of transverse positive faults that cause uplift of depocentres and basement highs (Milani & Thomaz Filho, 2000; Morais Neto et al., 2003). In the onshore Potiguar Basin, two phases of deformation were identified (Bezerra et al., 2020; Maia & Bezerra, 2020). The first phase occurred after rifting ceased, from the Late Cretaceous to the middle Miocene, and it is associated with an intra-plate strike slip regime with N-S trending compression. The second phase, from the middle Miocene to the present, is also characterized by a strike-slip stress regime with E-W to NW-SE compression that locally caused topographic doming and incipient basin inversion.

Preliminary cosmogenic isotope studies estimate low/moderate erosion rates (<0.1–10 m/Ma) on the highlands and sedimentary mesas and high (>11 m/Ma) erosion rates for the lowlands (Morais Neto et al., 2010, 2012). Morphostratigraphic studies also give estimates of long-term denudation rate during the Cenozoic–Quaternary in the range between 4 and 10 m/Ma (Peulvast et al., 2009; Morais Neto & Vasconcelos, 2010; Morais Neto et al., 2010) and 13 and 34 m/Ma in uplifted plateaus (Gurgel et al., 2013; Figure 1).

2.1 | Stratigraphy of the Pará-Maranhão, Barreirinhas and Ceará Basins

The Pará-Maranhão, Barreirinhas and Ceará Basins extend along the Brazilian continental shelf from the equator to 4°S, at longitudes between 47°W and 38°W (Figure 1). A system of extensional faults bound the Pará-Maranhão and the Barreirinhas Basins and an inverted basement high separates them from the Ceará Basin (Condé et al., 2007; Soares et al., 2007; Trosdtorf et al., 2007). This structural framework results in a similar Late Cretaceous–Neogene stratigraphic record in the Pará-Maranhão and Barreirinhas Basins and a clearly distinct one in the Ceará Basin.

In the Pará-Maranhão and Barreirinhas Basins, the Aptian rift sequence (Figure 2) lies directly above a sedimentary unit of probable Devonian age, beginning with terrestrial sandstones and shales that in the late Aptian and Albian pass on to marine to lagoonal limestones (Feijó, 1994: Soares et al., 2007; Trosdtorf Jr. et al., 2007). The Albian sequence is capped by a syn-rift unconformity dated at 102 Ma: this marks the transition between the rift and the post-rift sediments. The post-rift Cenomanian sediments form a mixed carbonate–siliciclastic sequence and they underlie a siliciclastic sequence that extend till the Maastrichtian. From the Maastrichtian onwards, the dominant feature of these basins is a carbonate platform, which has different facies, including proximal quartzose sandstones, high-energy carbonates and deep-water shales and turbiditic sandstones (Milani & Thomaz Filho, 2000; Trosdtorf et al., 2007). Two basic magmatic events affected both the Pará-Maranhão and Barreirinhas Basins: in the Late Cretaceous at 90 Ma and in the middle Eocene (Mizusaki et al., 2002).

The Ceará Basin is separated in several subbasins by basement highs, volcanic bodies and anticlines, which relate to wrench tectonics and basin inversion (Milani & Thomaz Filho, 2000; Morais Neto et al., 2003). The syn-rift sedimentary sequence started in the early-middle Aptian time directly above the basement rocks of the Borborema Province, accumulating up to 4000-m-thick continental deposits (Figure 2), which during the upper Aptian passed on to marine to shallow marine sediments (Condé et al., 2007). A regional unconformity between Aptian and Albian, at ca. 113 Ma, marks the transition to the post-rift sequence. From the Albian to the present, slope/deep-water shaly facies with subordinate sandstones and

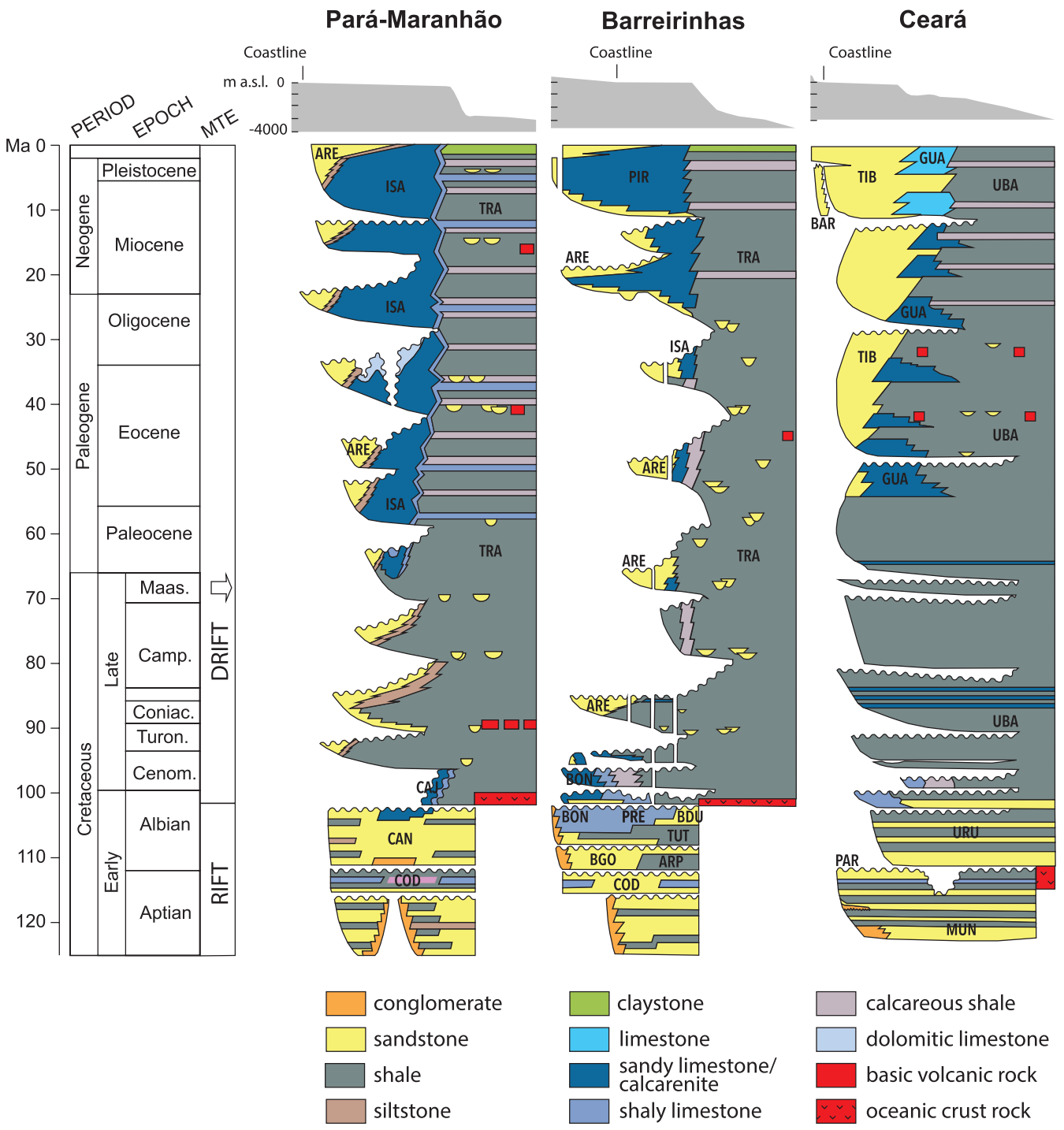

FIGURE 2 Stratigraphic charts of the Pará-Marañhao Basin (after Soares et al., 2007); of the Barreirinhas basin (after Trosdtorf Jr. et al., 2007); and of the Ceará basin (after Condé et al., 2007). Abbreviations – MTE: Main tectonic events; the arrow in the MTE column indicates the timing of the inversion deformation event in the Barreirinhas Basin. Pará-Marañhao basin: ARE: Areinhas Fm.; CAJ: Caju Gr.; CAN: Canárias Gr.; COD: Codó Fm.; ISA: Ilha de Santana Fm.; TRA: Travosas Fm. – Barreirinhas basin: ARE: Areinhas Fm.; ARP: Arpoador Fm.; BDU: Barro Duro Fm.; BGO: Bom Gosto Fm.; BON: Bonfim Fm.; COD: Codó Fm.; PIR: Pirabas Fm.; PRE: Preguiças Fm.; TRA: Travosas Fm.; TUT: Tutóia Fm. – Ceará basin: BAR: Barreiras Fm.; GUA: Guamaré Fm.; MUN: Mundaú Fm; PAR: Paracuru Fm.; TIB: Tibau Fm.; UBA: Ubarana Fm.; URU: Uruburetama Member.

limestones as proximal facies have been the dominant facies in this basin. In the mid-Eocene (ca. 44 Ma) and in the Oligocene (ca. 32 Ma), volcanic intrusive and effusive activity resulted in the emplacement of alkali basalts–phonolites and microgabbros (Mizusaki et al., 2002; Souza et al., 2022).

2.2 | Thermochronologic history of north-eastern Brazil

The low-temperature thermal evolution of the Borborema Province has been the focus of several thermochronologic studies, which have produced more than 100 apatite fission-track (AFT) ages on basement rocks (Figures 1 and 3; Cavalcante, 2006; Harman et al., 1998; Mojzeszowicz, 2009; Morais Neto et al., 2005–2006, 2008, 2009; Nóbrega et al., 2005; Turner et al., 2008). Different sampling approaches were employed to investigate the regional-scale thermal evolution (Harman et al., 1998; Mojzeszowicz, 2009), the thermochronologic signal across major tectonic boundaries (Cavalcante, 2006; Nóbrega et al., 2005) or the burial due to sedimentary covers and regional cooling events (Morais Neto et al., 2005–2006, 2008, 2009, Turner et al., 2008). All these studies have found a very long thermal record that extends across the entire Mesozoic and the Cenozoic from over 300 Ma until 40 Ma with only one AFT age younger than 40 Ma. The AFT age distribution has two main clusters (Figure 3): the largest one centres at ca. 90 Ma, which is shortly after rifting, and the smaller one centres around ca. 270 Ma. The largest cluster extends towards the present until ca. 20 Ma with a potential minor cluster of ages at ca. 50 Ma, and towards the past until about 230 Ma with a potential minor cluster at ca. 150 Ma. All AFT samples show reduced confined track lengths with mean values in the range 11–13 μm.

The wide range of AFT ages in the Borborema Province indicates that since the Early Cretaceous, only locally heating could reset the AFT record, and/or erosion was sufficient to exhume rocks from depths greater than the AFT closure depth. Moreover, the reduced AFT track lengths combined with the AFT ages indicate two main episodes of cooling since the Late Cretaceous: one immediately during the early Late Cretaceous (e.g. Harman et al., 1998) and one later in the Cenozoic until the present, from temperatures below 90°C to the surface (Morais Neto et al., 2009; Turner et al., 2008). The onset time for the second cooling event is not well resolved and varies between 50 and 25 Ma (Morais Neto et al., 2009; Turner et al., 2008). The amount and patterns of exhumation are very uncertain given that little is known about the geothermal gradient and its variation in space and time. Moreover, the possible geodynamic driver for uplift and exhumation remains also unclear, despite current views on north-eastern Brazil landscape evolution (Morais Neto & Vasconcelos, 2010; Sacek et al., 2019).

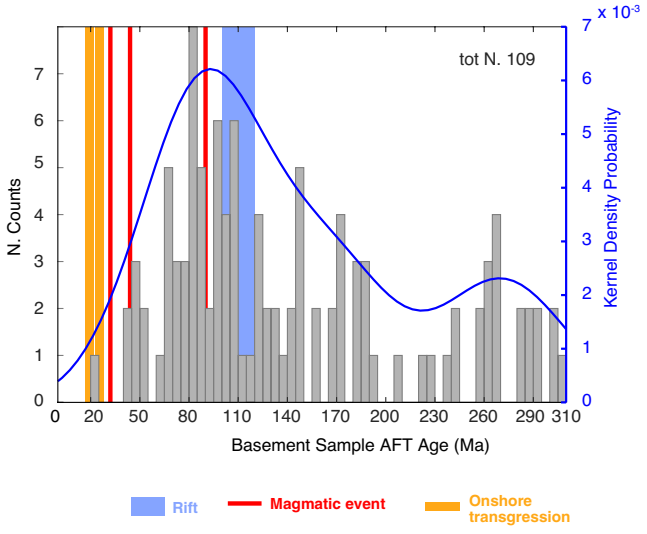

FIGURE 3 Histogram and distribution curve of the apatite fission-track ages from the basement rocks of the Borborema Province and Guaporé Craton from Harman et al. (1998), Cavalcante (2006), Nóbrega et al. (2005), Morais Neto et al. (2008, 2009), Turner et al. (2008) and Mojzeszowicz (2009).

3 | ANALYTICAL METHODS

This study database comprises newly available data that were analysed in 2003–2004 on 152 samples (Table 1) from cores of Petrobras™ along the Brazilian Equatorial Margin. Samples consist of both cores and cuttings, which have been treated for gross composition and heavy mineral analysis. Twenty-seven samples were processed for apatite fission-track analysis and thirteen of them (two cores and eleven cuttings) made available enough apatite grains for this study.

In the Pará-Maranhão Basin, samples were collected from Aptian–lower Oligocene sediments, and no samples from upper Oligocene–recent sediments are available (Figure 4). In the Barreirinhas and Ceará Basins, samples could be obtained from the entire sequence, ranging in age from the Aptian to the Recent.

3.1 | Gross composition

We analysed 133 thin sections from both cuttings and cores (Tables 1 and A1 in the Appendix S1). The thin sections were prepared after impregnation with blue epoxy resin from 29 core samples and 104 cuttings samples. The petrographic quantification was performed by counting 300 points in each thin section using the Gazzi–Dickinson modal point-counting method (Zuffa, 1985; Table A1 of the Appendix S1). The results were processed and plotted on Dickinson provenance detrital mode diagrams (Dickinson, 1985; Dickinson et al., 1983). Additional information on the quantification technique and on the indexes of the detrital mode diagrams is reported in the Appendix S1.

TABLE 1 Sampling framework.

No	Well	Drilled depth (m)	Elevation (m)	Core/cuttings	Depositional age range	GC	HM	AFT
1	BAR-01	288–318	−260	Cuttings	U.Olig./Rec.	GC1	HM1	
2		375–387	−352	Cuttings	Apt.	GC2	HM2	
3		780–810	−752	Cuttings	Apt.		HM3	
4		1503–1545	−1477	Cuttings	Apt.	GC4	HM4	
5		1857.6	−1830	Core	Apt.		HM5	
6	BAR-10	594–765	−650	Cuttings	U.Olig./Rec.	GC6	HM6	
7		1137–1155	−1124	Cuttings	Pal./L.Olig.	GC7	HM7	
8		1389–1485	−1400	Cuttings	M.Camp./ Maas.	GC8	HM8	
9		1545–1611	−1530	Cuttings	M.Camp./ Maas.	GC9	HM9	
10		2571–2586	−2480	Cuttings	U. Cen./L. Camp.	GC10	HM10	
11	BAR-20	705–750	−705	Cuttings	U. Cen./L. Camp.	GC11	HM11	
12		978–999	−950	Cuttings	U. Cen./L. Camp.		HM12	
13		1197–1212	−1155	Cuttings	U. Cen./L. Camp.	GC13	HM13	
14		1842.15	−1817	Core	Apt.	GC14	HM14	FT14
15	BAR-30	96–105	−76	Cuttings	U.Olig./Rec.	GC15	HM15	FT15
16		519–564	−516	Cuttings	M.Camp./Maas.	GC16	HM16	FT16
17		2247–2274	−2226	Cuttings	Apt.	GC17	HM17	FT17
18		2535–2553	−2500	Cuttings	Apt.	GC18	HM18	
19		2745–2757	−2726	Cuttings	Apt.	GC19	HM19	
20	BAR-31	342–441	−380	Cuttings	U.Olig./Rec.	GC20	HM20	
21		495–585	−520	Cuttings	U.Olig./Rec.	GC21	HM21	FT21
22		630–693	−627	Cuttings	Pal./L.Olig.	GC22	HM22	
23		759–777	−737	Cuttings	M.Camp./Maas.	GC23	HM23	
24		2805–2823	−2750	Cuttings	Apt.	GC24	HM24	
25	BAR-40	444–516	−423	Cuttings	Pal./L.Olig.	GC25	HM25	
26		642–696	−658	Cuttings	Pal./L.Olig.	GC26	HM26	FT26
27		993–1032	−973	Cuttings	M.Camp./Maas.	GC27	HM27	
28		1117.6	−1091	Core	U. Cen./L. Camp.	GC28	HM28	
29		1180.9	−1154	Core	U. Cen./L. Camp.	GC29	HM29	
30		2456.3	−2429	Core	Apt.	GC30	HM30	
31	CEA-36	381–408	−353	Cuttings	U.Olig./Rec.	GC31	HM31	
32		1116–1146	−1093	Cuttings	U.Olig./Rec.	GC32	HM32	
33		2637.4	−2610	Core	Apt.	GC33	HM33	
34		2898–2934	−2883	Cuttings	Apt.	GC34	HM34	
35	CEA-40	375–402	−351	Cuttings	U.Olig./Rec.	GC35	HM35	FT35
36		801–825	−786	Cuttings	U.Olig./Rec.	GC36	HM36	
37		1122–1158	−1096	Cuttings	U.Olig./Rec.	GC37	HM37	FT37
38		1752–1761	−1726	Cuttings	Pal./L.Olig.	GC38	HM38	
39		2580–2604	−2566	Cuttings	Apt.	GC39	HM39	
40		2857.1	−2833	Core	Apt.	GC40	HM40	
41		3474–3495	−3401	Cuttings	Apt.	GC41	HM41	
42	CEA-43	615–687	−576	Cuttings	U.Olig./Rec.	GC42	HM42	
43		1062–1110	−1051	Cuttings	U.Olig./Rec.	GC43	HM43	

(Continues)

TABLE 1 (Continued)

No	Well	Drilled depth (m)	Elevation (m)	Core/cuttings	Depositional age range	GC	HM	AFT
44		1674–1698	−1656	Cuttings	U.Olig./Rec.	GC44	HM44	
45		1878–1908	−1826	Cuttings	Pal./L.Olig.	GC45	HM45	
46		2076–2142	−2086	Cuttings	Pal./L.Olig.	GC46	HM46	
47		2649–2676	−2626	Cuttings	Apt.	GC47	HM47	
48		3384–3405	−3366	Cuttings	Apt.	GC48	HM48	
49	CEA-45	405–603	−475	Cuttings	U.Olig./Rec.	GC49	HM49	FT49
50		1389–1395	−1362	Cuttings	U.Olig./Rec.	GC50	HM50	
51		1551–1653	−1564	Cuttings	U.Olig./Rec.	GC51	HM51	FT51
52		1851–1881	−1834	Cuttings	Pal./L.Olig.	GC52	HM52	FT52
53		2214–2313	−2204	Cuttings	Apt.	GC53	HM53	FT53
54		2673–2787	−2640	Cuttings	Apt.	GC54	HM54	
55	CEA-48	2262–2370	−2254	Cuttings	M.Camp./Maas.	GC55	HM55	
56		3048.5	−3027	Core	Apt.	GC56	HM56	
57		3637.8	−3617	Core	Apt.	GC57	HM57	
58	CEA-50	2365.1	−2351	Core	U.Olig./Rec.	GC58	HM58	
59		2400–2451	−2416	Cuttings	U.Olig./Rec.	GC59	HM59	
60		2487.5	−2474	Core	U.Olig./Rec.	GC60	HM60	FT60
61		2550–2601	−2566	Cuttings	U.Olig./Rec.	GC61	HM61	
62		2901–3000	−2936	Cuttings	Pal./L.Olig.	GC62	HM62	
63	PAMA-10	3354–3372	−3336	Cuttings	Pal./L.Olig.	GC63	HM63	
64		3540–3564	−3516	Cuttings	Pal./L.Olig.	GC64	HM64	
65		4189.5	−4166	Core	Apt.	GC65	HM65	
66	PAMA-20	2094–2163	−2072	Cuttings	M.Camp./Maas.	GC66	HM66	
67		2535–2553	−2507	Cuttings	M.Camp./Maas.	GC67	HM67	
68	PAMA-25	1764–1788	−1733	Cuttings	Pal./L.Olig.	GC68	HM68	
69		2230.4	−2203	Core	Apt.	GC69	HM69	FT69
70		2480.2	−2453	Core	Apt.	GC70	HM70	
71		3079.9	−3053	Core	Apt.	GC71	HM71	
72	PAMA-30	1353–1443	−1358	Cuttings	Pal./L.Olig.	GC72	HM72	
73		2370–2379	−2338	Cuttings	Apt.	GC73	HM73	FT73
74		2571–2583	−2548	Cuttings	Apt.	GC74	HM74	FT74
75		3180–3189	−3163	Cuttings	Apt.	GC75	HM75	
76		3498–3510	−3478	Cuttings	Apt.	GC76	HM76	
77	PAMA-38	1191–1206	−1165	Cuttings	Pal./L.Olig.	GC77	HM77	
78		1218–1239	−1210	Cuttings	U. Cen./L. Camp.	GC78	HM78	
79		1263–1275	−1250	Cuttings	U. Cen./L. Camp.		HM79	
80		1630.7	−1606	Core	Apt.	GC80	HM80	
81		1881.9	−1857	Core	Apt.	GC81	HM81	
82		2969.1	−2944	Core	Apt.	GC82	HM82	
83		3302.4	−3277	Core	Apt.	GC83	HM83	
84		3829.7	−3805	Core	Apt.	GC84	HM84	
85	PAMA-39	1440–1458	−1404	Cuttings	Pal./L.Olig.	GC85	HM85	
86		1611–1674	−1599	Cuttings	Pal./L.Olig.	GC86	HM86	

TABLE 1 (Continued)

No	Well	Drilled depth (m)	Elevation (m)	Core/cuttings	Depositional age range	GC	HM	AFT
87		1854–1872	−1814	Cuttings	Pal./L.Olig.	GC87	HM87	
88		2485.8	−2455	Core	M.Camp./Maas.	GC88	HM88	
89		3525–3528	−3497	Cuttings	U. Cen./L. Camp.		HM89	
90		3660–3675	−3654	Cuttings	U. Alb./M. Cen.		HM90	
91		3720–3729	−3699	Cuttings	U. Alb./M. Cen.		HM91	
92	PAMA-40	1344–1458	−1355	Cuttings	Pal./L.Olig.		HM92	
93		1464–1554	−1470	Cuttings	Pal./L.Olig.		HM93	
94		1866–1878	−1840	Cuttings	Pal./L.Olig.	GC94	HM94	
95		2893.15	−2873	Core	U. Cen./L. Camp.	GC95	HM95	
96		2894.6	−2874	Core	U. Cen./L. Camp.	GC96	HM96	
97		3342–3402	−3318	Cuttings	U. Cen./L. Camp.	GC97	HM97	
98	PAMA-41	1224–1260	−1212	Cuttings	Pal./L.Olig.		HM98	
99		1329–1338	−1292	Cuttings	U. Cen./L. Camp.		HM99	
100		1680.1	−1652	Core	U. Cen./L. Camp.		HM100	FT100
101		1824–1830	−1772	Cuttings	Apt.		HM101	
102		2103–2109	−2072	Cuttings	Apt.		HM102	
103		2252.15	−2224	Core	Apt.		HM103	FT103
104		2904–2907	−2812	Cuttings	Apt.		HM104	
105		3479.3	−3451	Core	Apt.		HM105	
106	PAMA-50	1810–1825	−1790	Cuttings	Pal./L.Olig.		HM106	
107		2000–2080	−2015	Cuttings	Pal./L.Olig.		HM107	
108	PAMA-60A	3400.8	−3370	Core	U. Cen./L. Camp.		HM108	
109	PAMA-60B	1728–1755	−1707	Cuttings	Pal./L.Olig.		HM109	
110	BAR-50	360–408	−353	Cuttings	U.Olig./Rec.	GC110	HM110	
111		528–546	−493	Cuttings	Apt.	GC111	HM111	
112		756–786	−703	Cuttings	Apt.	GC112	HM112	
113		1147.63	−1121	Core	Apt.	GC113	HM113	
114		1153.2	−1126	Core	Apt.	GC114	HM114	FT114
115		1266–1275	−1243	Cuttings	Apt.	GC115	HM115	
116		1785–1794	−1763	Cuttings	Apt.	GC116	HM116	
117		2319–2316	−2288	Cuttings	Apt.	GC117	HM117	
118		2769–2781	−2733	Cuttings	Apt.	GC118	HM118	
119		2847.6	−2824	Core	Apt.	GC119	HM119	
120	BAR-60	96–114	−80	Cuttings	U.Olig./Rec.	GC120	HM120	
121		324–360	−298	Cuttings	U.Olig./Rec.	GC121	HM121	
122		2997–3015	−2978	Cuttings	Apt.	GC122	HM122	
123		3090–3102	−3068	Cuttings	Apt.	GC123	HM123	
124	CEA-10	153–165	−136	Cuttings	U.Olig./Rec.	GC124	HM124	
125		480–498	−437	Cuttings	U.Olig./Rec.	GC125	HM125	
126		795–816	−782	Cuttings	Apt.	GC126	HM126	
127		1509–1530	−1487	Cuttings	Apt.	GC127	HM127	FT127

(Continues)

TABLE 1 (Continued)

No	Well	Drilled depth (m)	Elevation (m)	Core/cuttings	Depositional age range	GC	HM	AFT
128		2436–2457	−2417	Cuttings	Apt.	GC128	HM128	
129	CEA-15	186–225	−156	Cuttings	U.Olig./Rec.	GC129	HM129	FT129
130		600–624	−586	Cuttings	Apt.?	GC130	HM130	
131		852–873	−826	Cuttings	Apt.?	GC131	HM131	
132		1245–1269	−1236	Cuttings	Apt.?	GC132	HM132	
133		1419.9	−1396	Core	Apt.?		HM133	
134	CEA-20	438–498	−451	Cuttings	U.Olig./Rec.	GC134	HM134	FT134
135		612–648	−621	Cuttings	U.Olig./Rec.	GC135	HM135	
136		1026.15	−1002	Core	U. Alb./M. Cen.	GC136	HM136	FT136
137		1308.9	−1285	Core	U. Alb./M. Cen.	GC137	HM137	
138		2006.3	−1982	Core	U. Alb./M. Cen.	GC138	HM138	
139		2541–2565	−2526	Cuttings	Rift?	GC139	HM139	
140		2625–2646	−2606	Cuttings	Rift?	GC140	HM140	
141	CEA-30	951–1023	−891	Cuttings	U.Olig./Rec.	GC141	HM141	FT141
142		1166.8	−1143	Core	M.Camp./Maas.	GC142	HM142	FT142
143		1314–1344	−1296	Cuttings	M.Camp./Maas.	GC143	HM143	
144		1920–1947	−1896	Cuttings	Apt.	GC144	HM144	
145		2187–2235	−2111	Cuttings	Apt.	GC145	HM145	
146		2301–2331	−2276	Cuttings	Apt.	GC146	HM146	
147	CEA-33	282–297	−260	Cuttings	U.Olig./Rec.	GC147	HM147	
148		474–498	−436	Cuttings	U.Olig./Rec.	GC148	HM148	
149		609–663	−604	Cuttings	U.Olig./Rec.	GC149	HM149	FT149
150		930–969	−926	Cuttings	M.Camp./Maas.	GC150	HM150	FT150
151		1620.1	−1596	Core	Apt.	GC151	HM151	
152		2940–2958	−2926	Cuttings	Apt.	GC152	HM152	

Note: AFT, samples analysed for apatite fission-track age determination; GC, samples analysed for gross composition; HM, samples analysed for heavy mineral content.Depositional age ranges: Apt., Aptian–lower Albian; M.Camp./Maas., middle Campanian–Maastrichtian; Pal./L.Olig., Palaeocene–lower Oligocene; U.Alb./M.Cen., upper Albian–middle Cenomanian; U.Cen./L.Camp., upper Cenomanian–lower Campanian; U.Olig./Rec., upper Oligocene–Recent.

3.2 | Heavy mineral analysis

Heavy mineral analysis was performed on 152 heavy mineral mounts (Table 1). The details of the sample preparation are reported in the Appendix S1. Heavy minerals were obtained from the sample fraction with grain size between 2ϕ (250 μm) and 4ϕ (63 μm). The weights of the dry (2–4)ϕ fraction and heavy mineral fraction were tracked only for some of the samples (62 of 152 samples). The heavy minerals species were counted by the ribbon method (Gazzi et al., 1973) and different grain types were tabulated (i.e. transparents – excluding baryte, Mg/Fe carbonate, opaques and turbids) in order to identify about 200 transparent grains for each sample (Table A2 of the Appendix S1).

3.3 | Fission-track analysis

Apatite grains could be successfully separated from about 1 kg bulk samples (core and cuttings; Table 1). Samples for AFT analysis were prepared following a standard procedure that is detailed in the Appendix S1. AFT dates are reported in Table 2 together with other AFT data. AFT dates were calculated using the external detector and the zeta-calibration methods (Hurford & Green, 1983) with IUGS age standards (Durango, Fish Canyon and Mount Dromedary apatites; Hurford, 1990). The analyses were subjected to the χ^2 test to detect whether the data sets contained any extra-Poissonian error (Galbraith, 1981, 2005; Vermeesch, 2019). A χ^2 probability of less than 5% denotes a significant spread of single-grain dates. For comparison with the sample depositional age, the

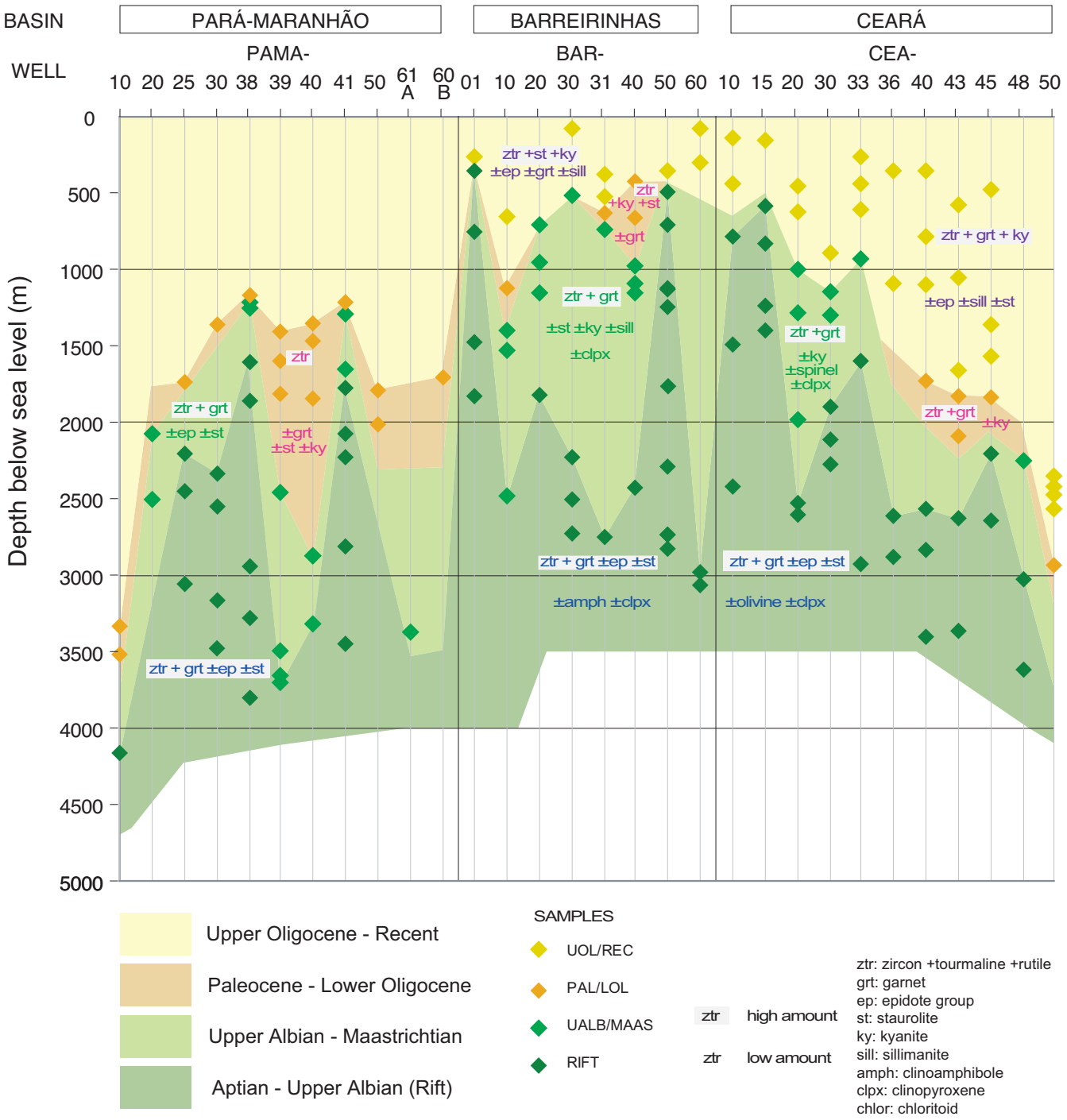

FIGURE 4 Main heavy mineral assemblages and position of the studied samples relative to depth along each well. Wells are ordered from NW to SE. The depth below sea level of the samples is the sample elevation relative to sea level, which differs from the mean drilled depth on average by 34 m and does not exceed 100 m (Table 1).

minimum ages of the grain age distributions were calculated following the approach of Vermeesch (2021): these are reported in Tables 2 and 3. The observed grain age distributions were decomposed into different component populations (or 'peak ages') by using the binomial peak-fitting method (Brandon, 1996; Brandon & Vance, 1992). The age and standard error of individual fitted peaks are reported in Table 3.

The lengths of horizontal confined fission tracks (CTL) were measured, and the mean of their distribution is reported in Table 2. Currently, the length of the fission-track etch pit (Dpar; Carlson et al., 1999) and the crystallographic orientation of CTLs (Donelick, 1999) are routinely measured, but at the time of data production those parameters were not measured and they could not be measured for this

TABLE 2 Apatite fission-track ages determined with the external detector method.

Well	Sample number	Core/ cuttings	Dep. Age range Ma	No. of crystals	Spontaneous ρ_s e+5 tr/cm^2	Spontaneous N_s tr	Induced ρ_i e+6 tr/ cm^2	Induced N_i tr	$P(\chi)^2$	Dosimeter ρ_d e+6 tr/cm^2	Dosimeter N_d tr	Central age ± 1σ Ma	Minimum age ± 1σ Ma	Mean confined track length ± std. err. µm	Std. dev.	No. of tracks measured	$\zeta_{CN5} \pm 1\sigma$
BAR-20	FT14	Core	125–102	25	1.53	145	0.78	742	79.6	1.17	5567	41.4 ± 3.8	45.9 ± 4.4	10.08 ± 0.26	2.18	68	366.46 ± 3.48
BAR-30	FT15	Cuttings	28–0	30	11.60	1254	1.66	1789	0.0	1.15	5450	137.0 ± 15.0	66.0 ± 10.0	n.d.	n.d.	n.d.	368.26 ± 4.85
BAR-30	FT16	Cuttings	78–66	24	8.82	939	1.90	2023	0.0	1.14	5414	105.8 ± 14.8	70.8 ± 4.3	n.d.	n.d.	n.d.	368.26 ± 4.85
BAR-30	FT17	Cuttings	125–102	30	1.06	88	1.24	1031	8.0	1.15	5481	16.4 ± 2.8	12.4 ± 4.6	9.21 ± 0.46	2.76	36	366.46 ± 3.48
BAR-31	FT21	Cuttings	28–0	24	7.97	822	1.70	1752	0.0	1.12	5342	103.8 ± 16.8	49.5 ± 8.5	n.d.	n.d.	n.d.	368.26 ± 4.85
BAR-40	FT26	Cuttings	66–28	30	11.56	1263	2.20	2402	0.0	1.11	5270	116.3 ± 13.5	51.0 ± 7.5	n.d.	n.d.	n.d.	368.26 ± 4.85
CEA-40	FT35	Cuttings	28–0	30	6.85	811	1.83	1543	0.5	1.12	5309	84.0 ± 8.6	76.3 ± 7.6	n.d.	n.d.	n.d.	355.5 ± 27.4
CEA-40	FT37	Cuttings	28–0	20	5.22	438	1.52	1277	73.2	1.08	5126	67.8 ± 4.0	68.3 ± 3.8	12.89 ± 0.15	1.22	69	368.26 ± 4.85
CEA-45	FT49	Cuttings	28–0	30	4.62	629	1.56	2124	0.0	1.05	5252	49.4 ± 5.7	36.2 ± 6.4	n.d.	n.d.	n.d.	355.5 ± 27.4
CEA-45	FT51	Cuttings	28–0	30	5.19	613	1.22	1441	0.4	1.06	5054	83.7 ± 6.1	59.8 ± 9.9	n.d.	n.d.	n.d.	368.26 ± 4.85
CEA-45	FT52	Cuttings	66–28	22	5.21	370	1.73	1227	0.9	1.06	5018	57.6 ± 5.7	55.0 ± 12.0	n.d.	n.d.	n.d.	368.26 ± 4.85
CEA-45	FT53	Cuttings	125–102	30	3.28	513	1.11	1734	0.0	1.09	5166	52.7 ± 5.2	39.0 ± 13.0	n.d.	n.d.	n.d.	368.26 ± 4.85
CEA-50	FT60	Core	28–0	20	2.90	190	1.19	782	87.6	1.08	5138	44.8 ± 5.0	48.5 ± 4.2	11.04 ± 0.15	2.52	84	366.46 ± 3.48
PAMA-25	FT69	Core	125–102	20	5.59	488	1.83	1597	33.1	1.03	4884	57.3 ± 3.5	52.0 ± 11.0	11.54 ± 0.16	1.63	100	366.46 ± 3.48
PAMA-30	FT73	Cuttings	125–102	20	0.88	61	1.27	881	21.5	1.02	4844	13.5 ± 2.1	14.5 ± 3.3	n.d.	n.d.	n.d.	366.46 ± 3.48
PAMA-30	FT74	Cuttings	125–102	20	0.59	52	1.86	1650	86.4	1.04	4964	6.0 ± 0.9	6.7 ± 1.1	10.94 ± 0.25	2.07	66	366.46 ± 3.48
PAMA-41	FT100	Core	96–78	5	4.91	35	1.07	76	65.6	1.00	4764	83.8 ± 17.2	86.0 ± 19.0	n.d.	n.d.	n.d.	366.46 ± 3.48
PAMA-41	FT103	Core	125–102	20	5.46	569	1.38	1444	13.3	0.99	4724	71.5 ± 4.2	72.0 ± 3.4	n.d.	n.d.	n.d.	366.46 ± 3.48
BAR-50	FT114	Core	125–102	20	4.78	374	1.28	999	38.8	0.96	4564	65.4 ± 4.2	66.7 ± 4.5	13.26 ± 0.15	1.53	100	366.46 ± 3.48
CEA-10	FT127	Cuttings	125–102	40	5.56	874	1.81	2836	0.2	0.91	4326	52.3 ± 3.0	45.0 ± 4.1	n.d.	n.d.	n.d.	366.46 ± 3.48
CEA-15	FT129	Cuttings	28–0	24	6.94	448	1.75	1131	80.3	0.90	4286	65.1 ± 3.8	65.7 ± 4.2	12.87 ± 0.19	1.91	100	366.46 ± 3.48
CEA-20	FT134	Cuttings	28–0	19	10.30	465	1.96	883	0.0	0.89	4246	91.6 ± 9.2	35.5 ± 8.8	n.d.	n.d.	n.d.	366.46 ± 3.48
CEA-20	FT136	Core	102–98	20	4.28	409	0.76	728	2.4	0.92	4366	93.4 ± 8.3	76.0 ± 21.0	n.d.	n.d.	n.d.	366.46 ± 3.48
CEA-30	FT141	Cuttings	28–0	40	9.13	1305	1.46	2085	0.0	0.88	4206	104.8 ± 8.1	58.7 ± 7.1	n.d.	n.d.	n.d.	366.46 ± 3.48
CEA-30	FT142	Core	78–66	13	4.87	170	1.11	387	51.0	0.97	4604	77.5 ± 7.3	78.5 ± 7.7	n.d.	n.d.	n.d.	366.46 ± 3.48
CEA-33	FT149	Cuttings	28–0	8	9.47	181	2.28	435	5.6	0.95	4516	70.7 ± 8.7	57.0 ± 14.0	n.d.	n.d.	n.d.	366.46 ± 3.48
CEA-33	FT150	Cuttings	78–66	20	7.58	421	1.70	947	31.1	0.94	4486	76.4 ± 5.1	71.7 ± 4.9	13.02 ± 0.18	1.83	100	366.46 ± 3.48

Note: Age (Ma) ± 1σ, central age and standard error in Ma; Dep. Age range, depositional age range; Mean confined track length (µm) ± std. err., length and standard error of the confined tracks; N_d, number of tracks on dosimeter; N_i, number of induced tracks (tr); No. of tracks measured, number of confined tracks; N_s, number of spontaneous tracks (tr); Std. dev., Standard deviation of the mean confined track lengths; $\zeta_{CN5} \pm 1\sigma$, ζ-calibration factor and standard error; ρ_d, dosimeter track density given as number of tracks (tr) over the size of the counting area; ρ_i, induced track density given as number of tracks (tr) over the size of the counting area; ρ_s, spontaneous track density given as number of tracks (tr) over the size of the counting area.Central ages are calculated using dosimeter glass CN5, a value of 0.5 for the 4π/2π geometry correction factor.

TABLE 3 Detrital age populations derived using Binomfit (Brandon, 1996).

#	Well	Sample	Drilled depth (m)	Dep. Age range Ma	*n*	Minimum age Age ± 1 s (Ma)	P1 Age ± 1 s (Ma) Fraction of grains	P2 Age ± 1 s (Ma) Fraction of grains	P3 Age ± 1 s (Ma) Fraction of grains	P4 Age ± 1 s (Ma) Fraction of grains	P5 Age ± 1 s (Ma) Fraction of grains
1	BAR-30	FT15	96–105	28–0	30	66.0 ± 10.0	–	62.8 ± 17.0 27.10%	–	150.6 ± 18.1 54.50%	335.7 ± 66.8 18.40%
2	BAR–30	FT16	519–564	78–66	24	70.8 ± 4.3	–	71.4 ± 7.1 72.30%	–	–	247.8 ± 39.4 27.70%
3	BAR–31	FT21	495–585	28–0	24	49.5 ± 8.5	–	64.1 ± 7.2 73.20%	–	–	290.4 ± 49.7 26.80%
4	BAR–40	FT26	642–696	66–28	30	51.0 ± 7.5	–	73.8 ± 7.8 60.80%	–	–	215.1 ± 32.6 39.2
5	CEA–40	FT35	375–402	28–0	30	76.3 ± 7.6	–	68.3 ± 16.2 60.00%	110.2 ± 28.6 40.00%	–	–
6	CEA–40	FT37	1122–1158	28–0	30	68.3 ± 3.8	–	67.7 ± 7.7 100.00%	–	–	–
7	CEA–45	FT49	405–603	28–0	30	36.2 ± 6.4	29.2 ± 10.6 34.90%	65.5 ± 12.3 65.10%	–	–	–
8	CEA–45	FT51	1551–1653	28–0	30	59.8 ± 9.9	–	57.0 ± 12.5 33.90%	98.5 ± 13.9 66.10%	–	–
9	CEA–15	FT129	186–225	28–0	24	45.0 ± 4.1	–	65.1 ± 3.8 100%	–	–	–
10	CEA–20	FT134	438–498	28–0	19	35.5 ± 8.8	–	76.1 ± 10.9 77.80%	–	163.2 ± 71.5 22.20%	–
11	CEA–30	FT141	951–1023	28–0	40	58.7 ± 7.1	–	57.8 ± 8.1 32.5	119.2 ± 21.1 44.30%	170.3 ± 46.7 23.20%	–
12	CEA–33	FT149	609–633	28–0	8	57.0 ± 14.0	–	70.7 ± 8.7 100%	–	–	–

Note: Dep. Age range, depositional age range; P1–P5, Population ages sorted from youngest to oldest; Age ± 1 s, Population age and standard error.

work. The measurements of Dpar and CTL crystallographic orientation are made to improve the time–temperature history reconstruction, and in sedimentary rocks, to improve the understanding of basin evolution (burial/exhumation). However, as this topic is beyond the scope of this study and regarding the overall limitations of our AFT data (e.g. low number of grains per sample and the extent of the potential source area), the time–temperature histories modelling will not be undertaken here. In the Appendix S1, we still report methods and results of time–temperature modelling that was done for samples with enough CTL and a clear reset signal (cf. Section 5.1).

4 | RESULTS

4.1 | Gross composition

The detrital modes of the samples correspond to the provenance fields of stable craton, transitional continental, recycled orogen and mixing among these groups. A magmatic arc contribution appears in two samples only (Figure 5; GC65 and CG97).

The dominant composition of the samples from the Pará-Maranhão Basin is arkosic to subarkosic corresponding to the field of transitional continental (Figure 5),

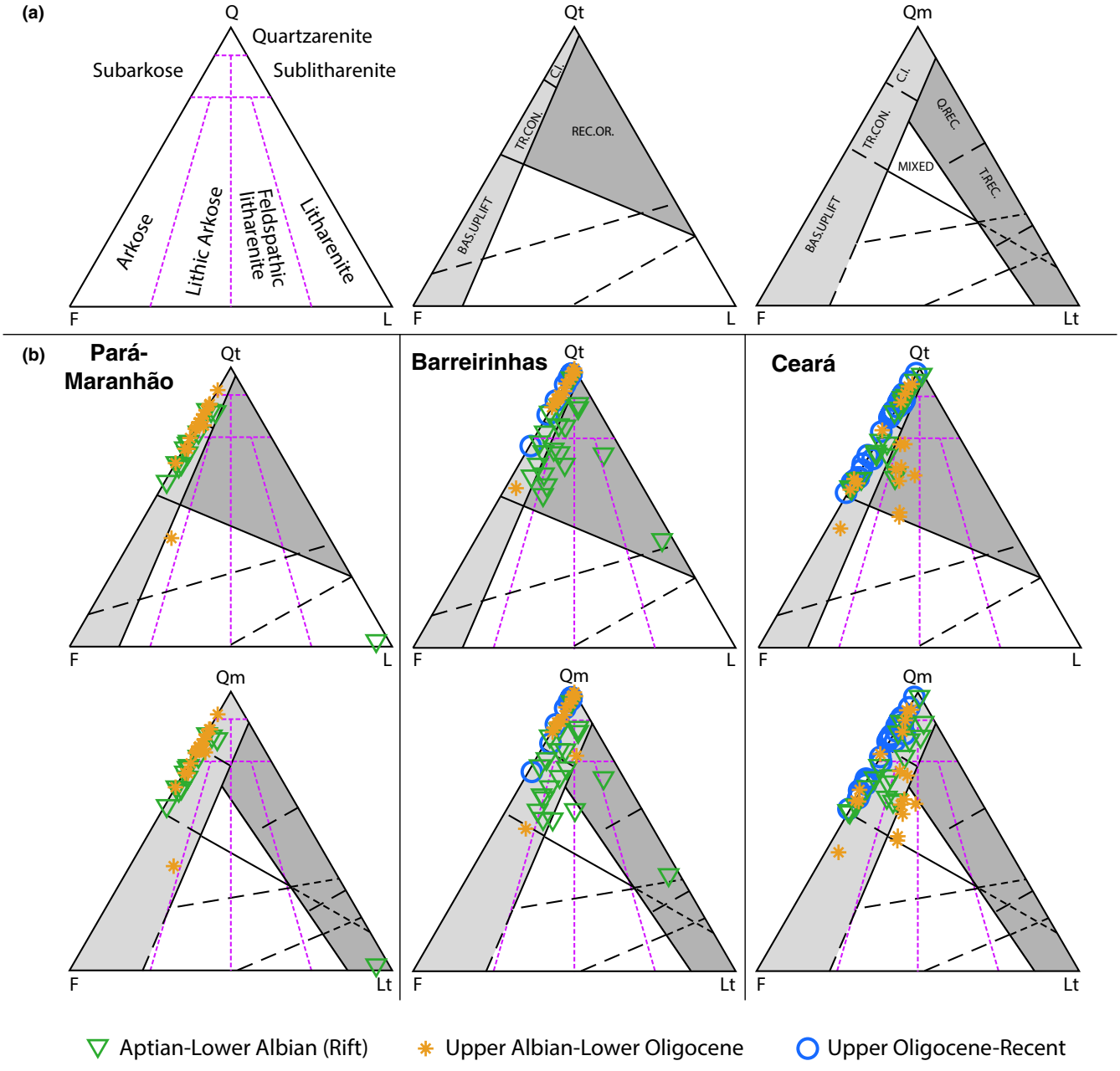

FIGURE 5 (a) Folk (1968) diagram for sandstone composition and Dickinson (1985) diagrams for sandstone provenance. BAS. UPLIFT, Basement uplift; C.I., Craton interior; Q.REC, Quartzose recycled; REC.OR, Recycled orogenic; T.REC., Transitional Recycled; TR.CONT., transitional continent. (b) Dickinson diagrams with the studied samples organized by basin and by depositional age.

indicating a provenance from eroded igneous and high-grade metamorphic terrains, with a trend to increasing quartzose composition towards the Palaeogene. A remarkable exception to this general composition is represented by a volcanic conglomerate from the Aptian–lower Albian (Rift) of the Pará-Maranhão Basin, related to intra-basinal volcanism.

The provenance of the Barreirinhas Basin samples show important influence of the recycling from ancient orogenic terrains (Figure 5), represented by micaceous and microcrystalline quartz fragments, from low-grade metamorphic origin. The recycled orogenic influence is consistently shown in the samples from cores and cuttings of all the analysed sequences. This recycled orogenic contribution is dominant in the Rift samples, where it is superimposed to a transitional continental provenance. The samples from the Upper Albian to Recent tend to have a more quartzose composition. Overall, the provenance of the Barreirinhas samples indicates an increase in the quartzose component after the Aptian–lower Albian (Rift) as similarly observed for the Pará-Maranhão samples.

The composition of the samples from the Ceará Basin varies within a relatively wide range (Figure 5). Most samples, from Rift to Recent, have an almost arkosic-to-quartzose composition in the provenance fields of basement uplift and transitional continental. However, two additional compositional populations can be identified: a population with quartzose composition, which includes some of the Rift and of the lower Oligocene-to-Recent samples, and a population with a lithic–arkosic composition that falls in the fields of the cratonic, transitional continental and recycled orogenic provenance. These mixed samples are not only from the Rift but also from the Upper Albian to Recent. Such deviation from the quartz increasing trend in the Barreirinhas Basins is probably related to the recurrent tectonism observed in the Ceará area (Bezerra et al., 2020).

4.2 | Heavy minerals

In the analysed samples, the number of heavy mineral species varies between 2 and 14 in all samples (Figure 6). The Rift samples have most commonly 6–7 heavy mineral species and only two have more than 10 species, whereas several upper Oligocene–Recent samples have up to 14 mineral species (Figure 6). The weight percentage of the heavy minerals (HM/(2–4)ϕ) varies between <1% and 10% without clear correlations with either down-hole depth or time although the Rift samples with the highest heavy mineral weight percentage tend to be at shallower depths (Figure 6). The fraction of transparent minerals relative to the total heavy minerals is highly variable between 1% and >90%, and is highest in some of the Rift samples (Figure 6).

The Rift samples of the Pará-Maranhão Basin are characterized by a simple zircon, tourmaline, rutile (ztr) and garnet (+grt) assemblage with irregular occurrence of epidotes, locally in large amounts and of small amounts of staurolite and kyanite (Figure 7). This association changes in the upper Albian–lower Cenomanian up to the Middle Campanian–Maastrichtian (UA/LC to MC/M; Figure 8). During this interval, the ztr association becomes dominant, garnet decreases significantly and epidote appears locally in very small amounts, as well as staurolite and kyanite. In the Palaeocene–lower Oligocene (P/LO; Figure 8), the ztr association remains dominant, but staurolite and kyanite appear frequently and locally in large amounts.

In the Barreirinhas Basin, the Rift samples are characterized by a simple ztr + grt assemblage with irregular occurrences of small amounts of epidote, kyanite and staurolite (Figure 7). An exception to this common assemblage is a sample that contains no ztr and consists largely of garnet, clinoamphibole and clinopyroxene. From the upper Cenomanian–lower Campanian to the middle Campanian–Maastrichtian (UC/LC to MC/M in Figure 8), the ztr assemblage becomes dominant, the garnet is less abundant than in the earlier samples, sillimanite and pyroxene appear irregularly in low amounts and staurolite and kynate are present locally in larger amounts than earlier. From the Palaeocene–lower Oligocene (P/LO in Figure 8) to the Recent (Figure 9), the characteristic assemblage is given by ztr, staurolite and kyanite. Garnet is present only in small amounts or absent, while epidote and unstable minerals such as amphibole, clino- and ortho-pyroxene (bronzite) appear locally in elevated amounts. Monazite (± xenotime) is present almost in all samples in significant amounts.

In the Ceará Basin, the heavy mineral composition from the Rift to the lower Oligocene features a dominant ztr + grt assemblage with larger amounts of garnet after the Rift. Kyanite, staurolite, amphibole and pyroxene occur very irregularly and in very small amounts (Figures 7–9). Exceptions to this common composition are three Rift samples that contain large amounts of olivine and clino- and ortho-pyroxene. In the upper Oligocene–Recent, the heavy mineral assemblage changes abruptly to a ztr + grt and kyanite association with irregular but relatively large occurrences of epidote and sillimanite. Monazite (±xenotime) is present almost in all samples in significant amounts.

Overall, in the Rift samples of all basins, the heavy mineral composition features a dominant ztr + grt assemblage with irregular, locally large, amounts of epidote

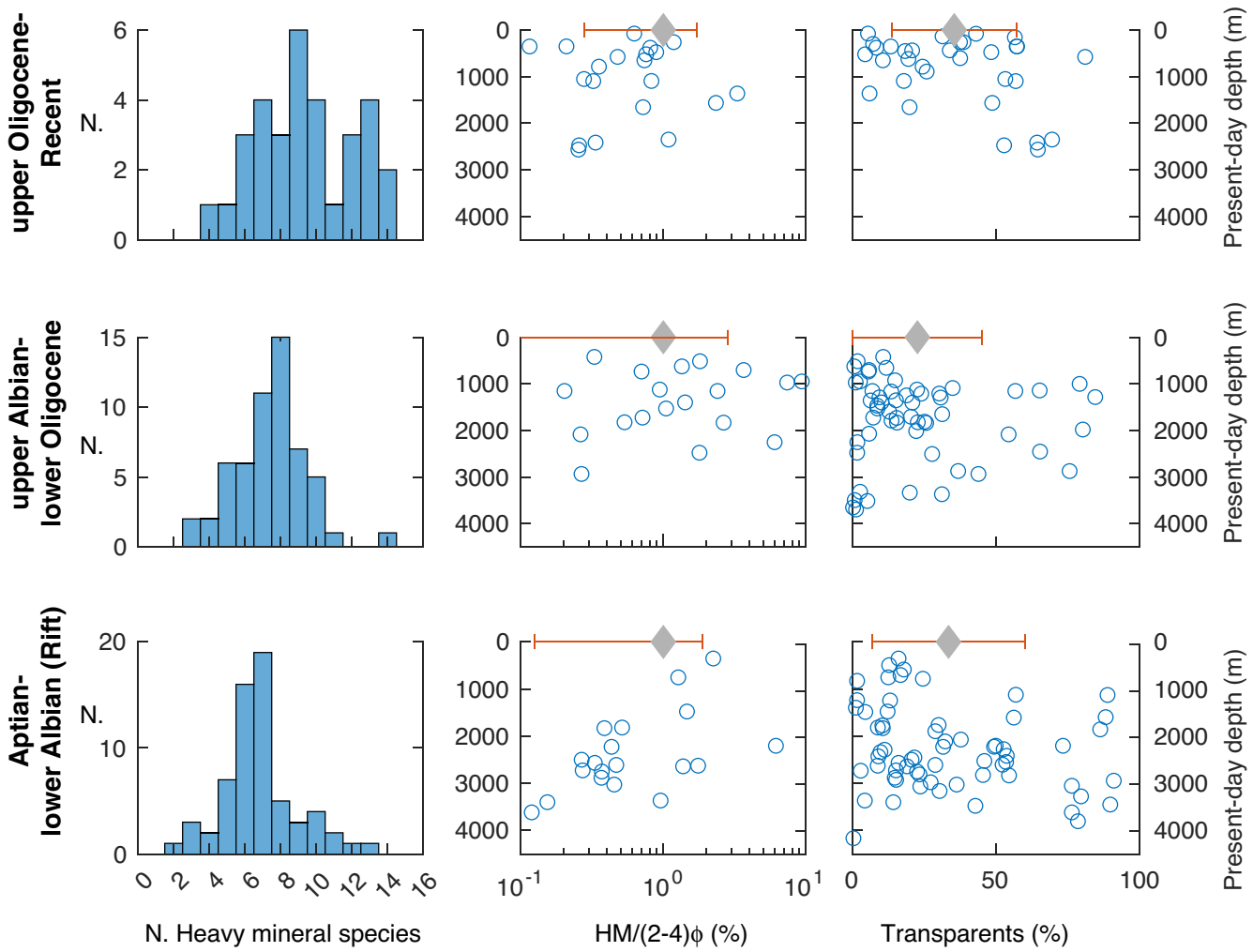

FIGURE 6 Left: bar diagram of the number (N.) of heavy mineral species for different depositional age intervals. Centre: blue circles indicate the heavy mineral fraction (HM/(2–4)ϕ) from the dried samples as a function of the down-hole depth for different depositional age intervals. Right: blue circles represent the down-hole percentages of transparent heavy mineral contents for different depositional age intervals. Grey diamond and red bar represent, respectively, the mean and standard deviation of the data shown in the plot. The present-day depth is the sample elevation relative to the mean sea level as reported in Table 1. Differences between sample elevation and mean drilled depth are average of 34 m and do not exceed 100 m.

and staurolite and rare, small amounts of kyanite. In the post-Rift samples, the ztr assemblage characterizes the Pará-Maranhão and Barreirinhas Basins, whereas the ztr + grt assemblage persists in the Ceará Basin. Significant amounts of kyanite appear frequently in the Barreirinhas and Ceará Basins and minor amounts in the Pará-Maranhão Basin. In the upper Oligocene–Recent samples, kyanite associated with a ztr + grt assemblage is dominant in the Ceará Basin, whereas staurolite and kyanite in combination with a ztr assemblage prevails in the Barreirinhas Basin.

In all basins, pyrite, baryte and iron-rich magnesite are present from low to very high quantity. Their features and distribution suggest an authigenic origin. Part of the anatase and brookite irregularly present may also be authigenic.

4.3 | Thermochronological data

All the datable grains in 27 samples were counted resulting in 19 to 40 dated apatites in 24 samples and 5 to 13 dated apatites in 3 samples (Table 3). The low number of grains reflects most likely the small sample size. Central AFT ages vary between 7 and 137 Ma and minimum ages between 7 and 86 Ma (Table 3; Figure 10). Statistical analysis of the data by the χ^2 test (Galbraith, 1981) shows a broad dispersion of single-grain ages in 13 of 27 samples. The samples that pass the χ^2 test have age distributions consistent with single populations, and these include all the Pará-Maranhão (PAMA) samples, two of the Barreirinhas (BAR) samples (FT14 and FT103) and six of the Ceará (CEA) samples (FT37, FT60, FT129, FT142, FT149 and FT150). The dispersed samples contain two-to-three age

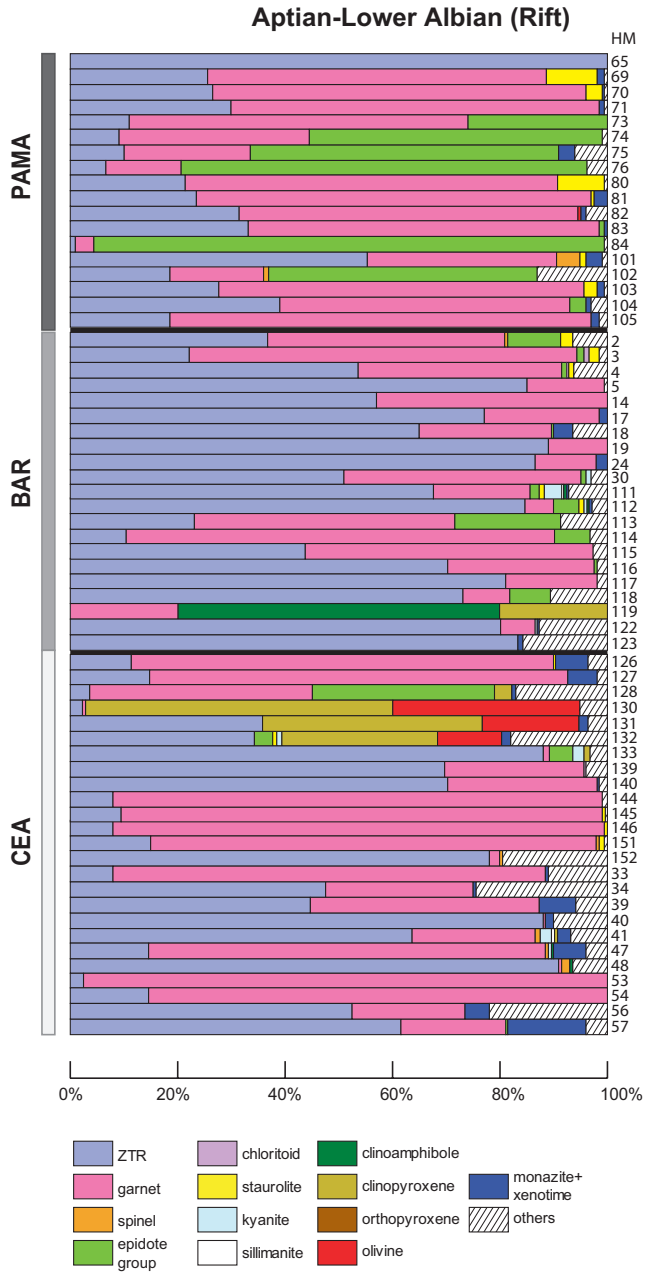

FIGURE 7 Bar diagrams of heavy mineral percentage in the samples from the Aptian–lower Albian samples. The bar stack is down-hole irrespectively of the well position; thus, the upper bars represent the shallower samples. Sample numbers are indicated in the HM column on the right side of the bar stack. Two thick black lines separate samples from different basins that are indicated by the vertical grey bars on the left. CEA: Ceará Basin, BAR: Barreirinhas Basin; PAMA: Pará-Marañhao Basin. ZTR: zircon + tourmaline + rutile.

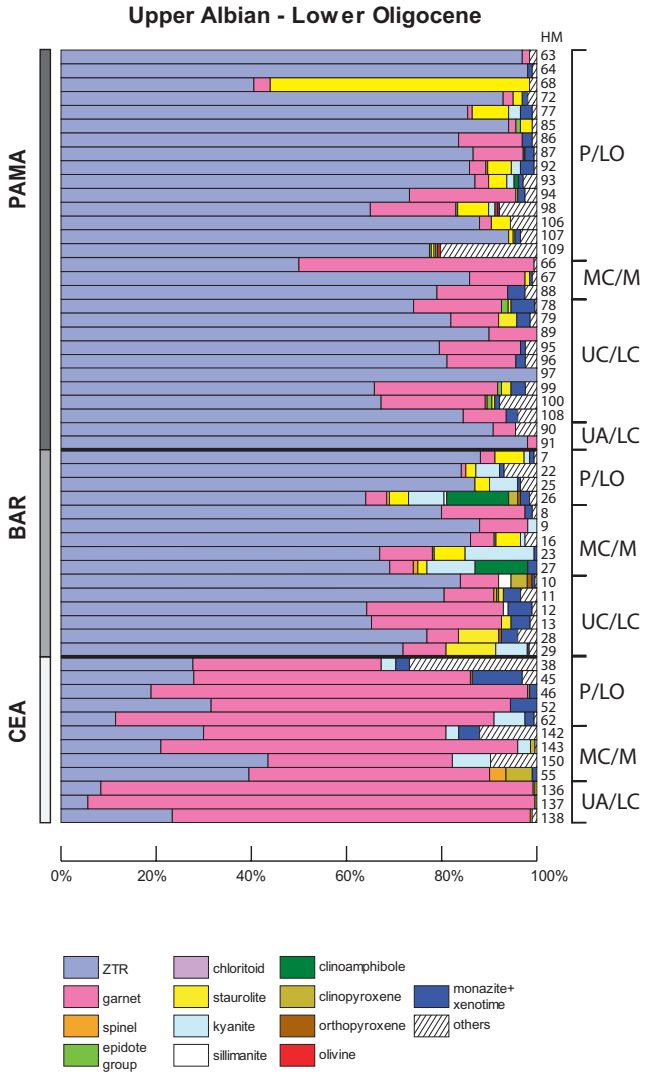

FIGURE 8 Bar diagrams of heavy mineral percentage in the samples from the upper Albian–lower Oligocene samples. The bar stack is down-hole irrespectively from the well position; thus, the upper bars represent the shallower samples. UA/LC: upper Albia–-lower Cenomanian; UC/LC: upper Cenomanian–lower Campanian; MC/M: middle Campanian–Maastrichtian; P/LO: Palaeocene–lower Oligocene. Sample numbers are indicated in the HM column on the right side of the bar stack. Two thick black lines separate samples from different basins that are indicated by the vertical grey bars on the left. CEA: Ceará Basin, BAR: Barreirinhas Basin; PAMA: Pará-Marañhao Basin. ZTR: zircon + tourmaline + rutile.

populations (Table 3; Figure 11). With the exception of sample FT49, the youngest and most common population vary between 57 and 76 Ma and the second most common populations varies between 99 and 119 Ma. Other older and less frequent populations centre between 151 and 170 Ma and between 215 and 336 Ma. Sample FT49 has a younger and smaller population including 35% of the grains and centring at 29 Ma, and an older population including the remaining grains and centring at 66 Ma.

Measurable CTLs were found in nine samples in a number varying between 36 and 100 CTL per sample (Table 2). Mean CTLs vary between 9.2 and 13.3 µm. Sample FT17 has the smallest mean CTL of 9.2 ± 0.5 and a central AFT age of 16.4 ± 2.8 Ma. Sample FT74 has the youngest AFT central age of 6.0 ± 0.9 Ma and mean CTL of 10.9 ± 0.3 µm.

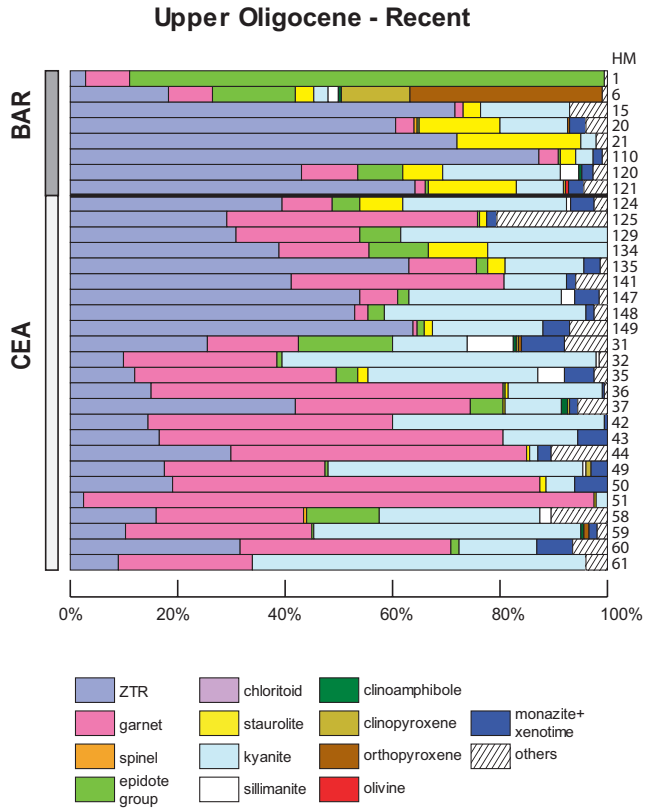

FIGURE 9 Bar diagrams of heavy mineral percentage in the samples from the upper Oligocene–Recent samples. The bar stack is down-hole irrespectively of the well position; thus, the upper bars represent the shallower samples. Sample numbers are indicated in the HM column on the right side of the bar stack. A thick black line separates samples from the different basins that are indicated by the vertical grey bars on the left. CEA: Ceará Basin, BAR: Barreirinhas Basin. ZTR: zircon + tourmaline + rutile.

The largest mean CTL of 13.3 ± 0.2 μm is shown by sample FT114 that has a central age of 65.4 ± 4.2 Ma.

5 | DISCUSSION

5.1 | Depth dependence of fission-track annealing

The annealing of fission tracks in apatite is controlled primarily by time, temperature and apatite composition (e.g. Reiners & Brandon, 2006). In detrital samples, the inherited, pre-depositional thermochronologic record plays also an important role (Ketcham et al., 1999). The temperature control on track annealing results in that detrital apatites in samples from a well show increasing degrees of annealing with depth: samples above a certain depth retain the pre-depositional fission-track record; deeper samples show a progressively higher degree of annealing, shorter mean confined track lengths and younger ages as the temperature increases down the well. Detrital samples sourced from rocks with different thermal histories have typically complex grain age distributions with multiple age populations, whereas detrital samples that, after burial and total annealing, cooled to temperatures below the fission-track partial annealing zone have commonly only one age population that represents the post-depositional cooling age. Thus, commonly non-reset detrital samples have complex age distributions with cooling ages older than the depositional age, whereas reset detrital samples have simple cooling age distributions centred at an age younger than the depositional age. A reset detrital sample can also feature multiple age populations due to different annealing behaviours, which become apparent when post-depositional cooling is slow and/or when apatites have very diverse compositions. Finally, the ability of discriminating between distributions with multiple- and single-age populations depends not only on the presence or absence of one or more age component but also on the number of dated grains per sample: that is, it depends on how the age distribution is sampled by the data. In fact, a low number of dated grains does not allow identifying all the potential age components in one sample but only the largest ones and may result in large uncertainties of the age and number of components (Vermeesch, 2004).

The complexity of the annealing process combined with the limitations of our data do not allow either to reconstruct the history or to quantify the degree of annealing of our samples. For the purpose of this study, it is sufficient to define which samples preserve a pristine detrital record and therefore to discriminate between samples that after deposition were non-reset and those that were partially-to-totally reset. Towards this goal, we first consider the AFT minimum age, which defines the youngest age component in an age distribution (Vermeesch, 2021). Then, we compare AFT minimum age and sample depositional age to discriminate three groups of samples (Figure 10). Finally, within each group, we elaborate on the degree of post-depositional annealing and age resetting based on other criteria including the AFT central age, the sample well depth, the age dispersion (whether samples pass the χ^2 test or fail it) and the mean CTL.

The three groups of samples are as follows:

- Group 1, including 10 samples with AFT minimum ages younger than the depositional age (Figure 10a). They all come from well depths greater than 1000 m and include: eight samples that pass the χ^2 test (Figure 10a,b), four samples (FT14, FT17, FT69 and FT74) with mean CTL in the 9–12 μm range and one sample (FT114) with a large CTL value of 13.3 μm (Figure 10c,d). The significantly reduced short mean confined track lengths, the AFT age, the modern great depth and the single-age

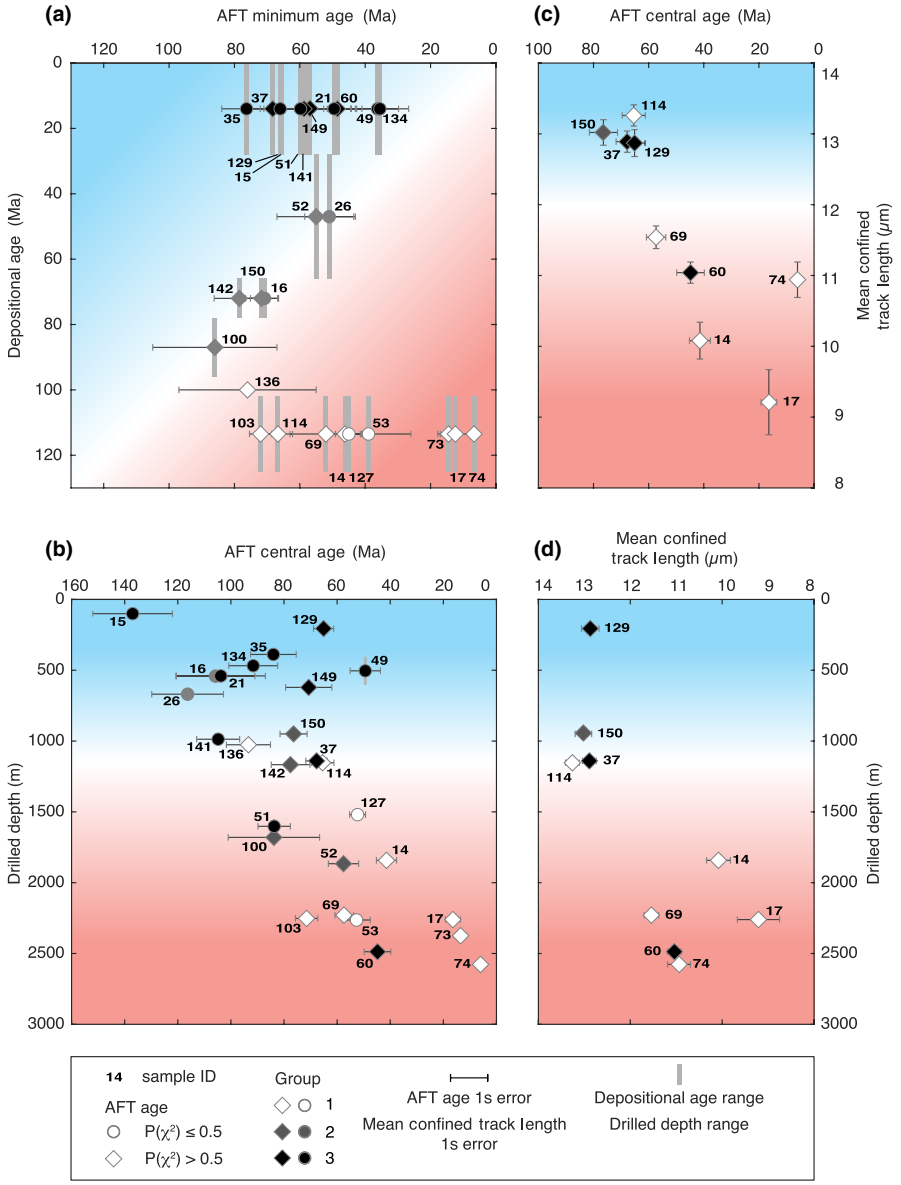

FIGURE 10 (a) Apatite fission-track (AFT) minimum ages against depositional age. Group 1: samples with AFT minimum age younger than the depositional age; Group 2: samples with minimum AFT age overlapping with the uncertainty of the depositional age; Group 3: samples with minimum AFT age older than the depositional age. (b) AFT central ages against mean drilled depth. The average difference between the drilled depths of individual samples is 54 m and the maximum difference is 198 m. Drilled depth and sample elevation relative to sea level are reported in Table 1: they differ on average by 34 m and differences do not exceed 100 m. Samples at depths shallower than 1200 m have AFT central ages that are older than their depositional age. (c) AFT central age against mean confined fission track length. Samples with AFT central ages younger than 60 Ma have mean confined track lengths shorter than 12 μm consistently with potential partial track annealing and age resetting. (d) Mean confined track length against drilled depth. Samples with mean confined track lengths shorter than 12 μm come from depths greater than 1200 m. Depositional and thermochronological data compared to present-day sample depth consistently indicate that most samples located at depths greater than 1200 m are potentially partially to fully annealed. Possible exceptions are samples 51 and 60 that have AFT central and minimum ages older than their depositional age. The blue area in all the diagrams represents the fission-track non-annealing zone, whereas the red area represents the fission-track partial to total annealing zone. Sample IDs are abbreviated to include only the numerals. The original sample ID includes also the letters FT for all the samples in this figure.

population of the majority of these samples indicate some degree of post-depositional annealing, which is particularly high in the deepest and youngest samples. The large mean CTL of sample FT114 combined with its 65-Ma-old AFT central age and Aptian depositional age could indicate partial-to-total annealing before 65 Ma followed shortly by cooling to low temperatures (Figure A2 in the Appendix S1).

- Group 2, including six samples with AFT minimum ages that overlap partly with the uncertainty of the

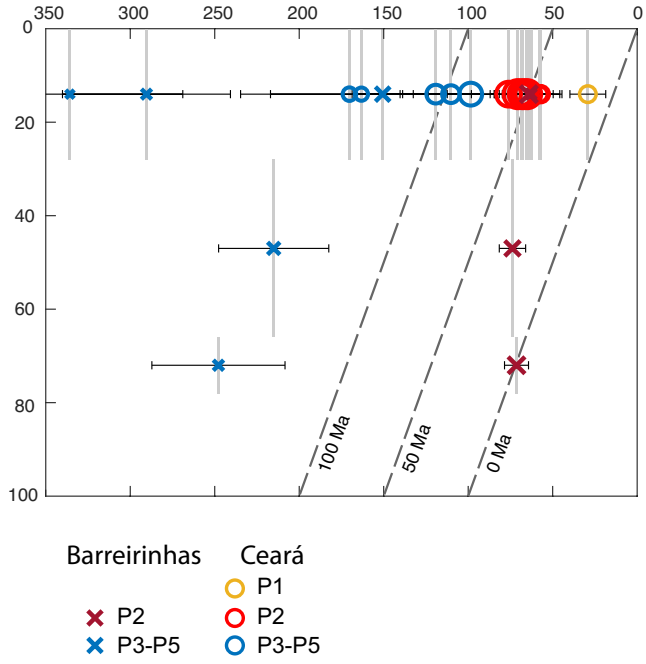

FIGURE 11 Detrital apatite fission-track age populations (P1–P5) derived with Binomfit (Brandon, 1996) plotted against depositional age. Dashed lines represent the lag time which is the time between deposition of the sediments and closure of the thermochronologic age (Bernet et al., 2001).

depositional age (Figure 10a). Two of these samples, FT16 and FT26, come from well depths of 542 m and 669 m and have overdispersed age distributions with central ages that are much older than their depositional ages (106 ± 15 Ma and 116 ± 14 Ma, respectively). These two samples could be non-reset and include grain ages with a short lag time relative to their deposition time. Alternatively, they could be partially reset and include only a minority of grains that record some degree of annealing. CTL distributions and independent constraints on maximum burial temperature would allow to discriminate between these alternative scenarios. Unfortunately, none of these data are available for these samples and we tentatively consider them as non-reset as this is the simplest explanation. The remaining samples (FT16, FT100, FT142 and FT150) come from a wide range of well depths from 950 m to 1866 m and have both minimum and central AFT ages that overlap with the depositional age. One of these samples (FT150) has a large mean CTL value of 13 μm, which would suggest little track length reduction for this samples. However, we consider all the samples currently at depths larger than 950 m and with an AFT minimum age similar to the depositional age as possibly affected by variable degree of annealing.

- Group 3, comprising 11 samples with AFT minimum ages older than the depositional age (Figure 10a). They all have depositional age that ranges between the upper Oligocene and the Recent. Nine of these samples are from well depths shallower than 1200 m (Figure 10b) and include two samples with mean CTL close to 13 μm (Figure 10c,d) and five samples with overdispersed ages. These nine samples could be non-reset or partially reset. Partial resetting would imply that after deposition they were buried within the AFT annealing zone shortly or at temperatures high enough to rejuvenate partly but not enough to become younger than their depositional age. However, given the mean CTLs of two of these samples, indicating no significant length reduction relative to typical mean CTLs of basement samples onshore (Cavalcante, 2006; Harman et al., 1998; Mojzeszowicz, 2009; Morais Neto et al., 2005–2006; Nóbrega et al., 2005; Turner et al., 2008), and their relatively young depositional age, the simplest explanation is that these samples are non-reset. The remaining two samples (FT51 and FT60) are potential outliers or could have undergone a complex history that the available data cannot resolve. FT51 preserves multiple age components that are much older than its Upper Oligocene–Recent depositional age, despite well depths around 1600 m. If this sample had a short time since deposition, then it might have preserved a detrital thermochronologic record due to short burial. Sample FT60 contains only one age population centred at around 45 Ma, which is older than its Upper Oligocene–Recent depositional age. However, this sample comes from a well depth of 2488 m, where temperatures are probably within the AFT partial annealing zone even if the geothermal gradient were as low as 20°C/km. Thus, this sample is certainly affected by some degree of AFT annealing despite the fact that its age is apparently non-reset. We speculate that this inconsistency may result from a possible erroneous designation of this sample as Upper Oligocene–Recent, whereas its true depositional age may be older. In conclusions, we consider as non-reset 10 samples from group 3, including sample FT51, although this should be considered with caution, and two samples from group 2 (FT16 and FT26).

The distribution with depth of non-reset and potentially partially reset ages is rather complex as shown in Figure 10. However, three sets of inferences are consistent with the majority of our data and these are as follows: i) the likely non-reset samples are at depths shallower than about 1 km; ii) samples deeper than about 1 km are reset to some degree; and iii) samples deeper than 2 km have strongly rejuvenated ages and very reduced mean confined track lengths (e.g. FT17, FT73 and FT74; Figure 10). Potential outliers, for instance, and most obviously sample FT60, testify to either poor data resolution or erroneous

designations. However, our data suggest that the shallower bound of the AFT partial annealing zone may lie at a depth of about 1 km and that partial age resetting occurs up to a depth of 2.5 km where our deepest and youngest AFT age is located (FT74; Figure 10). The young, non-dispersed age of this sample (FT74), together with its old depositional age (Aptian) and short mean confined track length (10.94 ± 2.5 μm), suggests vicinity to the deeper bound of the AFT partial annealing zone (Figure 10). Based on these inferences, we postulate that if we assume that the source area had similar annealing conditions as the basins, then in the last 100 Ma, which represent the time of the regional thermal event dominant throughout the Borborema Province (Morais Neto et al., 2009), at least 2.5 km of vertical erosion in the source areas would be necessary to expose fully reset AFT ages, more than 1 km would be necessary to expose partially reset ages and less than 1 km would result in the exposure of older, pre-100 Ma AFT ages.

5.2 | Erosion in the source area

Inferences on erosion in the source area are based on the analysis of the age components of the non-reset AFT samples only and on the assumption that age components represent the most important populations of cooling ages exposed in the source area at the time of erosion. Given the low number of datable grains in our samples, which does not exceed 40 grains per sample, the measured age distributions may only sample partially the true detrital age population. Therefore, we cannot affirm on the absence of age populations but only on their presence.

The youngest AFT age population (P1) in our samples centres at 29 ± 11 Ma, but this is present in only one sample (FT49) from the Ceará Basin (Figure 11; Table 3). In the modern source area of the Ceará, Barrerinhas and Pará-Maranhão basins, there are very few AFT ages that are Oligocene in age (Figures 1 and 3). Eocene and Oligocene intrusive and effusive magmatic phenomena affected the Ceará Basin and the structural high that separates it from the Potiguar Basin (Mizusaki et al., 2002; Souza et al., 2022). Thus, it remains unclear whether the 29-Ma-old detrital age population can be referred to local partial annealing due to high heat flow related to magmatism, a volcanic source or a source exhuming in the late Oligocene (Japsen et al., 2012; Jelinek et al., 2014; Morais Neto et al., 2009).

All the non-reset AFT samples in this study contain a detrital age population that centres around 70–60 Ma (P2; Figure 11; Table 3). This population is either the only population in the detrital samples with one age component or the largest in the majority of the samples with multiple age components. The 70- to 60-Ma-old detrital age populations are similar to several of the basement AFT ages along the Brazilian equatorial margin (Figures 1 and 3). These basement ages were interpreted as reflecting an increase in denudation during the Late Cretaceous–Early Palaeocene (Morais Neto & Vasconcelos, 2010), especially in the Ceará region, where a post-rift tectonic reactivation inverting inherited structures is clearly evident in the geologic record (Bezerra et al., 2020). Thus, the dominance of the 70–60 Ma age component in the detrital record provides further evidence in support of a major tectonic event that resulted in significant Late Cretaceous erosion of the source area. Based on our inferences on the relation of age resetting and sample depth as discussed in Section 5.1, assuming speculatively similar heat-flow conditions offshore and onshore, we can infer that since the Late Cretaceous the amount of vertical erosion of the source areas of the Barreirinhas and Ceará Basins is less than or up to 2.5 km.

Among the detrital AFT age populations older than 70–60 Ma, the first cluster of ages is around 100–90 Ma (P3; Figure 11; Table 3) that is close to the time of rifting (Condé et al., 2007; Soares et al., 2007) and therefore these AFT ages may represent exhumation of the rift shoulder. Finally, all samples from the Barreirinhas Basin show components older than 200 Ma and these age components are likely related to erosion of pre-Cretaceous Parnaíba sedimentary rocks or of basement rocks exposed to the west and south of the Parnaíba Basin that were not much affected by syn-to-post-rift tectonics.

While the 100- to 90-Ma-old AFT age component is present only in two (FT35 and FT141), possibly three (FT51) detrital samples (Table 3), in the basement rocks of the Borborema Province, it corresponds to the majority of ages (Figure 3). This difference may reflect a distinctive erosional record in the source areas of the Ceará and Barreirinhas Basins, which are dominated by a younger, Late Cretaceous event, in contrast to the erosional record of the rest of the Borborema Province, where the major event approaches the syn-rift stage. From this inference follows that our detrital record derives from an area that is only limitedly sampled by the available basement thermochronologic record. This is consistent with the observation that the AFT samples in the Borborema basement are located mostly in the central-eastern and southern sectors of this province and these sectors overlap only partly with the modern drainage area of the Ceará and Barreirinhas Basins. Alternatively, the dominant 70–60 Ma detrital signal could derive from a sample bias, which would result in that the relative proportions of the age clusters reflect different apatite concentrations in the source rocks and hydraulic sorting during transport, instead of variable erosion rates in space and/or time (e.g. Malusá et al., 2016). We have no constraints either on the apatite fertility of the

potential source rocks of the studied sandstones or on the processes that led to their deposition, thus we cannot resolve the different processes that control the relative proportions of the age components in our samples. However, we speculate that the fact that the 70–60 Ma detrital age component is commonly also the largest one could indicate that the older detrital age populations relate to source rocks that were actually eroding at lower rates relative to the source rocks of the ca. 70–60 Ma AFT ages and not to rocks depleted in apatites.

The lag time between the AFT age component of detrital samples and the depositional age can be used to derive inferences on the erosion rate of the source rocks and how this varies in time (e.g. Bernet et al., 2001; Figure 11). Given that the depositional age of our samples is only poorly resolved, we cannot extract precise information from upsection variations in the lag time. However, the available data indicate a lag time related to the 70–60 Ma age component that increases from Late Cretaceous to the Recent. Therefore, we can infer that our samples detect the signal of a source rock that was exhumed during the Late Cretaceous but, since then, was not affected by any other important exhumation event. Lag times increasing towards the Recent are consistent also with cannibalistic erosion of non-reset sediments (i.e. recycling) and the possible presence of rapid pulses of exhumation hidden in the 'thermochronological dead' zone (Ruiz et al., 2004), that is, after cooling below the closure temperature.

5.3 | Influence of burial diagenesis on the heavy mineral associations

The number of mineralogical species decreases for older samples (Figure 6). Authigenic minerals such as baryte and pyrite are present almost in all samples in very different amounts (Table 3). Slight corrosion features ('hacksaw terminations') have been found in some staurolite grains of samples HM 28 and 29 (depth of 1091 and 1154 m). Garnets showing well-developed faceting are also present in several deep-hole samples.

Traces of pristine unstable minerals (e.g. pyroxene and amphibole) are present in samples from old and deep sediments characterized by a ztr + grt assemblage. The weight percentages of transparent heavy minerals at progressive depths for all wells do not show a clear trend of decreasing amounts with depth. These data do not rule out that some diagenetic changes – as an effect of intrastratal dissolution – did occur but they do not allow estimating their effect on the heavy mineral distributions.

The heavy mineral content of sandstones is controlled by transport and diagenetic processes and also by chemical weathering of the source rocks as they were exposed at surface (e.g. Garzanti, 2017; Morton, 1999). Given the relatively low long-term erosion rates along the equatorial margin of Brazil, Mesozoic and pre-Mesozoic sedimentary covers and metamorphic rocks were exposed to weathering for long times. Thus, the high maturity of the older sequences could, at least in part, reflect significant modifications of the heavy mineral suites occurred before sediments erosion and transport. However, these or other processes were not strong enough to dissolve even most unstable heavy minerals species either in weathering profiles and/or during diagenesis. Thus, we infer that pre- and post-depositional modifications of the heavy mineral suites are likely relatively modest and do not compromise the ability to derive palaeogeographic and palaeotectonic inferences.

5.4 | Changes in provenance and implications for surface evolution

Petrographic and heavy mineral data show that during the rift phase, the sediment influx to the Pará-Maranhão, Barreirinhas and Ceará Basins derived from different source rocks (Figures 5 and 7). The sands delivered to the Pará-Maranhão Basin came from igneous and medium- to high-grade metamorphic terrains rich in garnet, epidote and staurolite (Figure 7). The detritus of the Barreirinhas Basin derived mainly from siliciclastic Palaeozoic cover sequences with a secondary contribution from basement rocks (Figure 7). The dominant cover sequences supplied lithic–arkosic-to-quartzose sands carrying a mature heavy mineral association dominated by the ultra-stable minerals, and igneous and medium- to high-grade metamorphic rocks, including locally paragneiss rich in aluminosilicate minerals, supplied arkosic sands rich mainly in garnet, epidote and staurolite and rarely in kyanite (Figures 5 and 7). The minor lithic component and the heavy mineral assemblage of the Ceará Basin suggest that the cover sequence was likely less dominant then in the Barreirinhas Basin and the basement source rocks were similar (Figures 5 and 7). Olivine and pyroxene in a few samples of the Ceará Basin could come from a local source of ultramafic magmatic rocks. The different provenance pattern is well justified by the modern onshore geological setting which shows the Parnaíba Basin and its sedimentary filling and Precambrian basement facing the Pará-Maranhão and Barreirinhas Basins, whereas Precambriam and Neoproterozoic crystalline basement rocks occur along the coast in front of the Ceará Basin (Figure 1). Sandstones of the rift phase underwent some diagenetic processes with corrosion and partial dissolution of feldspars and of some heavy mineral species such as not only staurolite but also garnet (in the Ceará Basin).

After the rift phase, from the Late Cretaceous until the early Oligocene, the principal composition and heavy

mineral assemblage varied in all the studied basins (Figures 5 and 8). The Pará-Maranhão Basin, and more evidently the Barreirinhas Basin, show an increasingly quartzose composition combined with a heavy mineral assemblage dominated by ultra-stable minerals and notably more mature than in the rift phase. In contrast to the Pará-Maranhão and Barreirinhas Basins, the Ceará Basin shows a slight enrichment in the lithic–arkosic component combined with increase in kyanite and disappearance of epidote. During this first post-rift phase, the appearance of significant amounts of kyanite and the decrease, almost disappearances, of epidote is a common feature of all three basins, suggesting that during this time the source of the moderately stable heavy minerals changed from medium- to high-grade metasedimentary and igneous rocks rich in garnet, epidote and staurolite, to dominantly high-grade metasedimentary rocks containing aluminosilicate minerals. These changes in provenance likely reflect major landscape alterations along the Brazilian equatorial margin in response to rock uplift and erosion. Evidence of uplift come from the sedimentary record in the Parnaíba, Araripe and Potiguar Basins (Figure 1) that fully emerged above sea level after the Cenomanian (e.g. Rossetti et al., 2013). Other lines of evidence supporting uplift come from the offshore stratigraphic record indicating syn-sedimentary inversion along transverse structures that especially affected the Ceará Basin and that lead to the uplift of structural highs (Milani & Thomaz Filho, 2000; Morais Neto et al., 2003). Erosion is indicated especially by the offshore thermochronologic record, which features the largest detrital AFT age populations at 70–60 Ma (Figure 11). Thus, uplift and erosion may have resulted in the emersion above sea level of new areas, for instance, the northern part of the Parnaíba Basin, and in the exposure in the drainage area of the Ceará Basin of source rocks that in the rift phase were likely only modestly exposed and that during the first post-rift phase started to supply significant amounts of lithic–arkosic detritus rich in garnet and aluminosilicate minerals. Moreover, uplift combined with erosion most likely led to drainage reorganization and resulted in a fluvial system partly similar to the modern one. The modern drainage system is characterized by two main features: a topographic high (Serra de Ibiapaba) separating the Parnaíba Basin from the Borborema Province, where the kyanite-bearing rocks are predominantly exposed, and by river branches that from the Parnaíba Basin directly tap into the Borborema Province locally cutting through the topographic high (near Crateús; C in Figure 1) and possibly bringing kyanite- and garnet-rich sands towards the Barreirinhas and Pará-Maranhão Basins.

Starting from the late Oligocene, the detrital influx changed in composition both in the Barreirinhas and Ceará Basins (Figures 6 and 9). In the Barreirinhas Basin, some samples had a larger arkosic component than during the late Cretaceous–Oligocene time, indicating provenance from the transitional continental field, and considerable amounts of minerals such as ortho- and clinopyroxene, amphibole and epidote, staurolite and kyanite. In the Ceará Basin, the lithic component decreased, and the composition shifted to quartzose–arkosic in combination with a sharp increase in kyanite and the reappearance of epidote and staurolite. The implications of this change in provenance are debatable. In the Araripe Basin (Figure 1), which includes the top of the Araripe Plateau around 300 km inland from the Ceará Basin, AFT data suggest up to 1.5 km of denudation in the last 30 Ma (Morais Neto et al., 2005–2006), although such amount may be overestimated (Morais Neto et al., 2010). According to Pessoa Neto (2003), such a recent stage of denudation would explain the siliciclastic influx observed in the Neogene sediments of the offshore Potiguar Basin (Figure 1). However, these interpretations have been recently challenged based on morpho-stratigraphic data indicating less than 600 m of post-Cenomanian surface uplift and mean erosion rates of 1 m/Ma (Peulvast & Bétard, 2021; Sacek et al., 2019). Our detrital AFT data do not detect significant Neogene detrital age populations (Figure 11), indicating that during this time, in the drainage areas of the basins of this study, vertical erosion must have been less than 1 km. However, most of our detrital thermochronologic data come from strata that could date back to the late Oligocene (Figure 11). Thus, it is possible that our data cannot resolve Neogene detrital signals. Moreover, our inference on the amount of erosion can only be applied to the source area of the basins in this study. However, this area cannot be determined exactly for the past and at present is located mostly to the west and north of the area discussed by Pessoa Neto (2003), Morais Neto et al. (2005–2006) and Peulvast and Bétard (2021). Thus, we suggest that the change in provenance since the late Oligocene detected by our sandstone petrographic composition but not by the thermochronologic data may be interpreted as related to either poor temporal resolution of the thermochronologic record or modest vertical erosion in the source area (less than 1 km) and to an expansion upstream of the drainage network resulting in larger exposures of rocks bearing aluminosilicate mineral. Modest vertical erosion combined with headwater expansion may have resulted partly in the removal of quartz-rich sedimentary covers and this could explain the shift towards more quartzose composition.

Figure 12 summarizes the major implication for the source area surface evolution. The major drainage reorganization and erosional event occurred after the

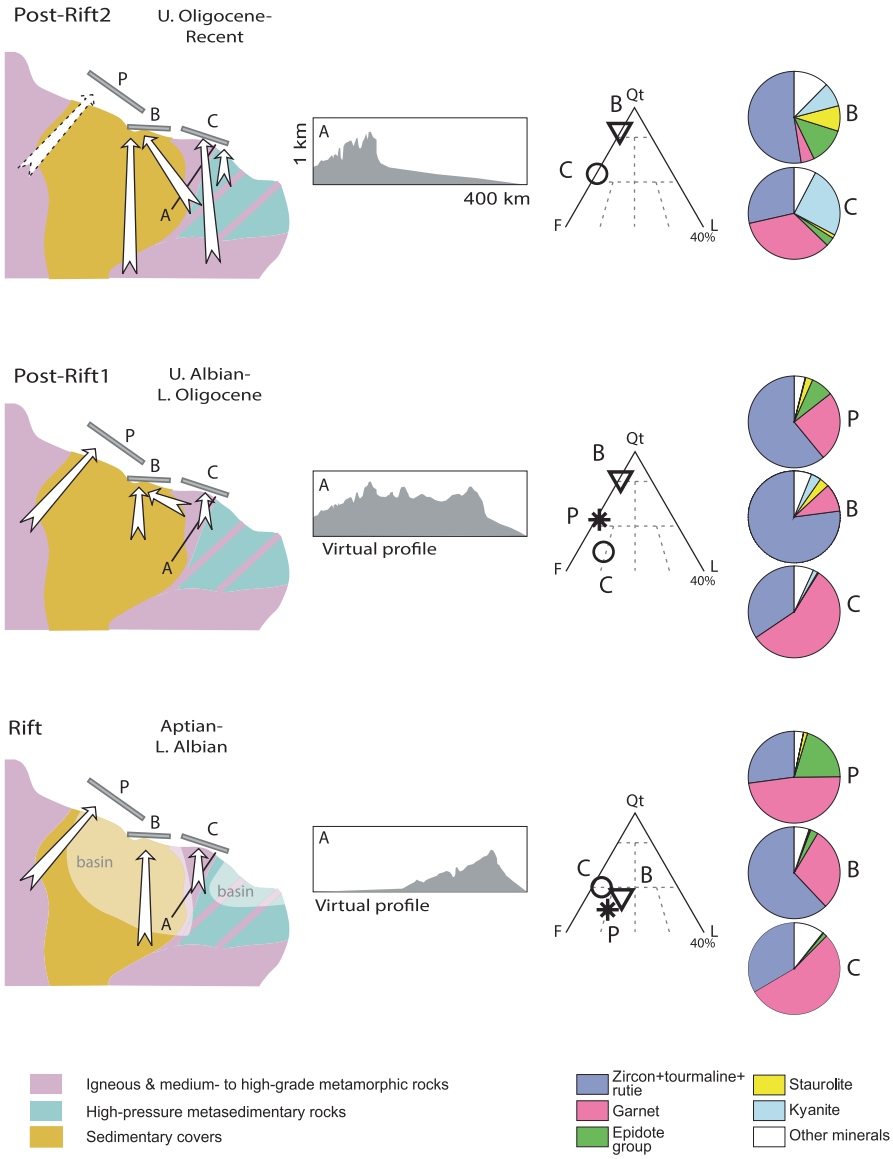

FIGURE 12 Schematic reconstruction of the changes in provenance and landscape as recorded by the detrital record of the Pará-Marañhao (P), Barreirinhas (B) and Ceará (C) Basins. Dickinson (QtFL) and pie diagrams show the means of the sandstone composition and of the main heavy minerals, respectively. 1. High-grade orthogneiss and granites; 2. high-grade paragneiss; and 3: siliciclastic rocks. A in Post-Rift 2 shows the location of the topographic profile shown in the inset to the right. A in Post-Rift 1 and Rift shows how a topographic profile on the shore of the Ceará basin might have looked back in the past.

Cenomanian, around 70 and 60 Ma. During this time, a new drainage network developed and carried abundant arkosic sands rich in aluminosilicate minerals and garnet mainly to the Ceará Basin and secondarily also to the Barreirinhas and Pará-Maranhão Basins. The new drainage network at this time was likely formed by relatively short rivers eroding the topographic high that formed in the Ceará region and during the Neogene these rivers may have expanded towards the continent interior. The dominance of the Late Cretaceous detrital age populations in the offshore record suggests that the total amount of erosion in the source area is in the order of 2–2.5 km since the Late Cretaceous and less than 1 km since the Late Oligocene.

The geodynamic mechanism that may have triggered the 70–60 Ma erosional event remains controversial. South of the study area, according to Japsen et al. (2012), a Campanian exhumation event may relate to far-field effects given by growth of the Andean orogen and a decline in spreading rate at the Mid-Atlantic Ridge. A change in relative plate motion has been invoked also by Harman et al. (1998) to explain the Late Cretaceous exhumation of the São Francisco and Guaporé cratons and the concurrent deformation of the western African continental margin. To explain the Late Cretaceous exhumation of the Borborema Province, Morais Neto et al. (2009) proposed thermal-isostatic uplift and magmatic underplating. Sacek et al. (2019) explained 70% of the post-rift regional uplift as resulting from the combined effect of differential denudation and flexural rebound of the lithosphere and the remaining 30% as thermal uplift induced by partial erosion of the base of the continental lithosphere underneath the Borborema Province. Our data, rather than revealing the geodynamic scenarios governing post-rift tectonic, provide some constraints on the maximum amount of

exhumation related to these events along the equatorial margin of Brazil and inform on the dynamics of the landscape evolution.

6 | CONCLUSIONS

This study demonstrated that the sediments deposited since the Early Cretaceous along the equatorial Brazilian margin are characterized by a dominantly arkosic composition and a pristine heavy mineral assemblage that testify to the progressive exhumation and exposure over larger areas of metasedimentary rocks.

During the rift stage, which lasted until the transition between Early and Late Cretaceous (ca. 100 Ma), erosion associated with uplift of the rift flank was moderate and not extensive. The syn-rift detrital supply to the Pará-Maranhão, Barreirinhas and Ceará Basins came from at least three different sources, including an igneous and high-grade metamorphic basement, subordinate metasedimentary rocks and siliciclastic sedimentary covers.

During the Late Cretaceous, around 70–60 Ma ago, a widespread change in the detrital signature occurred at the same time with a major drainage reorganization event in the source areas. This event resulted in a large recycling of the sedimentary cover rocks into the Pará-Maranhão and Barreirinhas Basins, in a source switch to moderately stable heavy minerals that derived dominantly from high-grade metasedimentary rock and in a lasting erosional event totalling up to 2–2.5 km of exhumation.

From the late Oligocene, the composition of the detrital supply has diversified with inputs of both quartzose and arkosic sands rich in kyanite and garnet but the exhumation record has not rejuvenated. Altogether, this indicates that the drainage divides have changed by headwater migration and piracy, resulting in possibly significant horizontal erosion but limited vertical erosion that has not exceeded 1 km.

ACKNOWLEDGEMENTS

We thank Alexis Derycke, Mauricio Parra and an anonymous reviewer for their constructive and insightful comments that improved this paper. Open access funding provided by Eidgenossische Technische Hochschule Zurich.

FUNDING INFORMATION

This research was funded under contract by Petrobras™.

CONFLICT OF INTEREST STATEMENT

There is no conflict of interest.

PEER REVIEW

The peer review history for this article is available at https://www.webofscience.com/api/gateway/wos/peer-review/10.1111/bre.12808.

DATA AVAILABILITY STATEMENT

The data that support the findings of this study are available in the Supplementary Material of this article.

ORCID

Maria Giuditta Fellin https://orcid.org/0000-0003-3545-3512

REFERENCES

Arthaud, M. H., Caby, R., Fuck, R. A., Dantas, E. L., & Parente, C. V. (2008). Geology of the northern Borborema Province, NE Brazil and its correlation with Nigeria, NW Africa. In R. J. Pankhurst, R. A. J. Trouw, B. B. Brito Neves, & M. J. De Wit (Eds.), *West Gondwana: Pre-Cenozoic correlations across the South Atlantic region* (Vol. *29*, pp. 49–67). Geological Society, London, Special Publications. https://doi.org/10.1144/SP294.4

Arthaud, M. H., Fuck, R. A., Dantas, E. L., Santos, T. J. S., Caby, R., & Armstrong, R. (2015). The Neoproterozoic Ceará group, Ceará central domain, NE Brazil: Depositional age and provenance of detrital material. New insights from U-Pb and Sm-Nd geochronology. *Journal of South American Earth Sciences*, *58*, 223–237. https://doi.org/10.1016/j.jsames.2014.09.007

Belton, D. X., Brown, R. W., Kohn, B. P., Fink, D., & Farley, K. A. (2004). Quantitative resolution of the debate over antiquity of the central Australian landscape: Implications for the tectonic and geomorphic stability of cratonic interiors. *Earth and Planetary Science Letters*, *219*, 21–34. https://doi.org/10.1016/S0012-821X(03)00705-2

Bernet, M., Zattin, M., Garver, J. I., Brandon, M. T., & Vance, J. A. (2001). Steady-state exhumation of the European Alps. *Geology*, *29*(1), 35–38.

Bezerra, F. H., Castro, D. L., Maia, R. P., Sousa, M. O. L., Moura-Lima, E. N., Rossetti, D. F., Bertotti, G., Souza, Z. S., & Nogueira, F. C. C. (2020). Post-rift stress field inversion in the Potiguar Basin, Brazil - implications for T petroleum systems and evolution of the equatorial margin of South America. *Marine and Petroleum Geology*, *111*, 88–104.

Brandon, M. T. (1996). Probability density plot for fission-track grain-age samples. *Radiation Measurement*, *26*, 663–676.

Brandon, M. T., & Vance, J. (1992). New statistical methods for analysis of fission- track grain-age distributions with applications to detrital zircon ages from the Olympic subduction complex, western Washington state. *American Journal of Science*, *292*, 565–636.

Campbell, K. E., Frailey, C. D., & Romero-Pittman, L. (2006). The pan-Amazonian Ucayali peneplain, late Neogene sedimentation in Amazonia, and the birth of the modern Amazon River system. *Palaeogeography, Palaeoclimatology, Palaeoecology*, *239*, 166–219.

Carlson, W. D., Donelick, R. A., & Ketcham, R. A. (1999). Variability of apatite fission-track annealing kinetics: I. *Experimental*

Results: The American Mineralogist, *84*, 1213–1223. https://doi.org/10.2138/am-1999-0901

Cavalcante, A. S. A. (2006). *Evolução termocronológica do sistema de falhas Senador Pompeu – CE*. (Master dissertation). Universidade Federal do Rio Grande do Norte, Natal (53 pp).

Condé, V. C., Cunha, C. C., Pessoa Neto, O. C., Roesner, E. H., Morais Neto, J. M., & Dutra, D. C. (2007). Bacia do Ceará. *Boletim de Geociências da Petrobras, Rio de Janeiro*, *15*(2), 347–355.

Cordani, U. G., Brito Neves, B. B., Fuck, R. A., Porto, i. R., Thomaz Filho, A., & Cunha, F. M. B. (2009). Estudo preliminar de integração do Pré-Cambriano com os eventos tectônicos das bacias sedimentares brasileiras (Republicação). *Boletim de Geociências da Petrobras, Rio de Janeiro*, *17*(1), 133–204.

Dickinson, W. R. (1985). Interpreting provenance relations from detrital modes of sandstones. In G. G. Zuffa (Ed.), *Provenance of arenites* (pp. 333–362). D. Reidel Publishing Company. https://doi.org/10.1007/978-94-017-2809-6_15

Dickinson, W. R., Beard, L. S., Brakenridge, G. R., Erjavec, J. L., Ferguson, R. C., Inman, K. F., Knepp, R. A., Lindberg, F. A., & Ryberg, P. T. (1983). Provenance of north American Phanerozoic sandstones in relation to tectonic setting. *GSA Bulletin*, *94*(2), 222–235.

Donelick, R. A. (1999). Crystallographic orientation dependence of mean etchable fission-track length in apatite: An empirical model and experimental observations. *American Mineralogist*, *76*, 83–91.

Feijó, F. J. (1994). Bacia de Barreirinhas. *Boletim de Geociências da Petrobras, Rio de Janeiro*, *8*(1), 103–109.

Folk, R. L. (1968). *Petrology of sedimentary rocks*. Hemphill Publishing Company.

Galbraith, R. F. (1981). On statistical models for fission tracks counts. *Mathematical Geology*, *13*, 471–478.

Galbraith, R. F. (2005). *Statistics for fission track analysis*. CRC Press.

Garcia, X., Julià, J., Nemocó, A. M., & Neukirch, M. (2019). Lithospheric thinning under the Araripe Basin (NE Brazil) from a long-period magnetotelluric survey: Constraints for tectonic inversion. *Gondwana Research*, *68*, 174–184.

Garzanti, E. (2017). The maturity myth in sedimentology and provenance analysis. *Journal of Sedimentary Research*, *87*, 353–365. https://doi.org/10.2110/jsr.2017.17

Gazzi, P., Zuffa, G. G., Paganelli, L., & Gandolfi, G. (1973). Provenienza e dispersione litoranea delle sabbie delle spiagge adriatiche fra le foci dell'Isonzo e del Foglia: inquadramento regionale. *Memorie Della Societa Geologica Italiana*, *12*, 1–37.

Góes, A. M., & Feijó, F. J. (1994). Bacia do Parnaíba. *Boletim de Geociências da Petrobras, Rio de Janeiro*, *8*(1), 57–67.

Gurgel, S. P., Bezerra, F. H., Corrêa, A. C., Marques, F. O., & Maia, R. P. (2013). Cenozoic uplift and erosion of structural landforms in NE Brazil. *Geomorphology*, *186*, 68–84.

Harman, R., Gallagher, K., Brown, R., Razza, A., & Bizzi, L. (1998). Accelerated denudation and tectonic/geomorphic reactivation of the cratons of northeastern Brazil during the late Cretaceous. *Journal of Geophysical Research – Solid Earth*, *103*(11), 27091–27105.

Heine, C., Zoethout, J., & Müller, R. D. (2013). Kinematics of the South Atlantic rift. *Solid Earth*, *4*, 215–253. https://doi.org/10.5194/se-4-215-2013

Hurford, A. J. (1990). Standardization of fission track dating calibration: Recommendation by the Fission Track working Group of the I.U.G.S. Subcommission on Geochronology. *Chemical Geology*, *80*, 171–178.

Hurford, A. J., & Green, P. F. (1983). A guide to fission track dating calibration. *Chemical Geology (Isotope Geosciences Section)*, *1*, 285–317.

Japsen, P., Chalmers, J. A., Green, P. F., & Bonow, J. M. (2012). Elevated, passive continental margins: Not rift shoulders, but expressions of episodic, post-rift burial and exhumation. *Global and Planetary Change*, *90-91*, 73–86. https://doi.org/10.1016/j.gloplacha.2011.05.004

Jelinek, A. R., Chemale, F., Jr., van der Beek, P. A., Guadagnin, F., Cupertino, J. A., & Viana, A. R. (2014). Denudation history and landscape evolution of the northern East-Brazilian continental margin from apatite fission-track thermochronology. *Journal of South American Earth Sciences*, *54*, 158–181.

Ketcham, R. J., Donelick, R. A., & Carlson, W. D. (1999). Variability of apatite fission-track annealing kinetics: III. Extrapolation to geologic time scales. *American Mineralogist*, *48*, 1235–1255.

Lima, M. G. (2008). *A História do Intemperismo na Província Borborema Oriental, Nordeste do Brasil: Implicações Paleoclimáticas e Tectônicas*. (Doctoral Thesis). Univ. Fed. Rio Grande do Norte.

Maia, R., & Bezerra, F. H. (2020). *Structural geomorphology in Northeastern Brazil*. Springer International Publishing. https://doi.org/10.1007/978-3-030-13311-5_2

Malusá, M. G., Resentini, A., & Garzanti, E. (2016). Hydraulic sorting and mineral fertility bias in detrital geochronology. *Gondwana Research*, *31*, 1–19. https://doi.org/10.1016/j.gr.2015.09.002

Matos, R. M. D. (1992). The northeastern Brazilian rift system. *Tectonics*, *11*, 766–791.

Milani, E. J., & Thomaz Filho, A. (2000). Sedimentary basins of South America. In U. G. Cordani, E. J. Milani, T. homaz Filho, & D. A. Campos (Eds.), *Tectonic evolution of South America* (pp. 389–449). 31st International Geological Congress, Rio de Janeiro.

Mizusaki, A. M. P., Thomaz Filho, A., Milani, E. J., & Césero, P. (2002). Mesozoic and Cenozoic igneous activity and its tectonic control in the northeastern region of Brazil, South America. *Journal of South America Earth Sciences*, *15*, 183–198.

Mojzeszowicz, A. G. (2009). *Evolução da tectônica ruptil no Nordeste do Brasil baseada na termocronologia por traço de fissão em apatita*. (Master thesis). UNESP, Rio Claro, Brasil, (64 pp).

Morais Neto, J. M., Green, P. F., Karner, G. D., & Alkmim, F. F. (2008). Age of the Serra do Martins Formation, Borborema Plateau, northeastern Brazil: Constraints from apatite and zircon fission track analysis. *Boletim de Geociências da Petrobras*, *16*(1), 23–52.

Morais Neto, J. M., Hegarty, K. A., & Karner, G. D. (2005–2006). Abordagem preliminar sobre paleotemperatura e evolução do relevo da Bacia do Araripe, Nordeste do Brasil, a partir da análise de traços de fissão em apatita. *Boletim de Geociências da Petrobras*, *14*(1), 113–118.

Morais Neto, J. M., Hegarty, K. A., Karner, G. D., & Alkmim, F. F. (2009). Timing and mechanisms for the generation and modification of the anomalous topography of the Borborema Province, northeastern Brazil. *Marine and Petroleum Geology*, *26*(7), 1070–1086.

Morais Neto, J. M., Pessoa Neto, O. C., Lana, C. C., & Zalán, P. V. (2003). Bacias Sedimentares Brasileiras: Bacia do Ceará. *Fundação Paleontológica Phoenix*, *57*, 1–6.

Morais Neto, J. M., & Vasconcelos, P. M. (2010). Thermochronological controls on the exhumation of the Eastern Borborema Province, Northeastern Brazil. In *Conference: 2010 AGU Meeting of the Americas at: Foz Do Iguaçu, Brazil Volume: EOS Trans. AGU, (Vol. 91). Meet. Am. Suppl., Abstract T12A-03*.

Morais Neto, J. M., Vasconcelos, P. M., & Stone, J. (2010). Cosmogenic 10Be constraints on the denudation history of the Borborema Province, Northeastern Brazil. In *Conference: 2010 AGU Meeting of the Americas at: Foz do Iguaçu, Brazil Volume: EOS Trans. AGU, 91(26), Meet. Am. Suppl., Abstract T21B-13*.

Morais Neto, J. M., Vasconcelos, P. M., Stone, J., & Lima, M. D. (2012). *Denudation patterns in the Borborema Province, northeastern Brazil: Constraints from cosmogenic ^{10}Be isotope analysis*. IUGS/AGC, 34th International Geological Congress, Brisbane, Proceedings, 2722.

Morton, A. C. (1999). Processes controlling the composition of heavy mineral assemblages in sandstones. *Sedimentary Geology*, *124*, 3–29.

Motta Garcia, M. D. G., Santos, T. J. S., & Amaral, W. S. (2014). Provenance and tectonic setting of neoproterozoic supracrustal rocks from the Ceará central domain, Borborema Province (NE Brazil): Constraints from geochemistry and detrital zircon ages. *International Geology Review*, *56*(4), 481–500. https://doi.org/10.1080/00206814.2013.875489

Nascimento, M. A., Galindo, A. C., & Medeiros, V. C. (2015). Ediacaran to Cambrian magmatic suites in the Rio Grande do Norte domain, extreme northeastern Borborema Province (NE of Brazil): Current knowledge. *Journal of South American Earth Sciences*, *58*, 281–299. https://doi.org/10.1016/j.jsames.2014.09.008

Nóbrega, M. A., Sá, J. M., Bezerra, F. H., Hadler Neto, J. C., Iunes, P. J., Guedes, S., Tello Saenz, C. A., Hackspacher, P. C., & Lima-Filho, F. P. (2005). The use of apatite fission track thermochronology to constrain fault movements and sedimentary basin evolution in northeastern Brazil. *Radiation Measurements*, *39*, 627–633. https://doi.org/10.1016/j.radmeas.2004.12.006

Pessoa Neto, O. C. (2003). Estratigrafia de Sequências da Plataforma mista neogênica na Bacia Potiguar, Margem Equatorial Brasileira. *Revista Brasileira de Geociencias*, *33*, 263–278.

Peulvast, J.-P., & Bétard, F. (2021). Morphostratigraphic constraints and low temperature thermochronology: Lessons from a review of recent geological and geomorphological studies in Northeast Brazil. *Journal of South American Sciences*, *111*, 103464. https://doi.org/10.1016/j.jsames.2021.103464

Peulvast, J.-P., Bétard, F., & Lageat, Y. (2009). Long-term landscape evolution and denudation rates in shield and platform areas: A morphostratigraphic approach. *Géomorphologie Relief, Processes, Environment*, *15*, 95–108. https://doi.org/10.4000/geomorphologie.7540

Reiners, P. W., & Brandon, M. T. (2006). Using thermochronology to understand orogenic erosion. *Annual Review of Earth and Planetary Sciences*, *34*, 419–466.

Rossetti, D. F., Bezerra, F. H., & Dominguez, J. M. (2013). Late Oligocene-Miocene transgressions along the equatorial and eastern margins of Brazil. *Earth Science Reviews*, *123*, 87–112.

Ruiz, G. M. H., Seward, D., & Winkler, W. (2004). Detrital thermochronology - a new perspective on hinterland tectonics, an example from the Andean Amazon Basin, Ecuador. *Basin Research*, *16*, 413–430. https://doi.org/10.1111/j.1365-2117.2004.00239.x

Sacek, V., Morais Neto, J. M., Vasconcelos, P. M., & Carmo, I. O. (2019). Numerical modelling of weathering, erosion, sedimentation and uplift in a triple junction divergent margin. *Geochemistry, Geophysics, Geosystems*, *20*(5), 2334–2354. https://doi.org/10.1029/2018GC008124

Soares, E. F., Zalán, P. V., Figueiredo, J. J. P., & Trosdtorf, I., Jr. (2007). Bacia do Pará-Maranhão. *Boletim de Geociências da Petrobras, Rio de Janeiro*, *15*(2), 321–329.

Souza, Z. S., Vilalva, J. C. J., Dantas, E. L., Lafon, J.-M., Silveira, F. V., & Oliveira, J. L. (2022). Petrogenesis and tectonics of Eocene-Oligocene phonolites of Mecejana, Ceará, NE Brazil: The role of the Fernando de Noronha fracture zone, equatorial Atlantic. *Journal of Petrology*, *63*, 1–32. https://doi.org/10.1093/petrology/egac051

Trosdtorf, I., Jr., Zalán, P. V., Figueiredo, J. J. P., & Soares, E. F. (2007). Bacia do Barreirinhas. *Boletim de Geociências da Petrobras, Rio de Janeiro*, *15*(2), 331–339.

Turner, J. P., Green, P. F., Holford, S. P., & Lawrence, S. R. (2008). Thermal history of the Rio Muni (West Africa)-NE Brazil margins during continental breakup. *Earth and Planetary Science Letters*, *270*(3–4), 354–367.

Vasconcelos, P. M., Farley, K. A., Stone, J., Piacentini, T., & Fifield, L. K. (2019). Stranded landscapes in the humid tropics: Earth's oldest land surfaces. *Earth and Planetary Science Letters*, *519*, 152–164. https://doi.org/10.1016/j.epsl.2019.04.014

Vermeesch, P. (2004). How many grains are needed for a provenance study? *Earth and Planetary Science Letters*, *224*, 441–451.

Vermeesch, P. (2019). Statistics for fission track thermochonrology. In: Fission-track thermochronology and its application to geology. In *Springer textbooks in earth sciences, geography and environment* (pp. 109–122). Springer. https://doi.org/10.1007/978-3-319-89421-8_6

Vermeesch, P. (2021). Maximum depositional age estimation revisited. *Geoscience Frontiers*, *12*, 843–850.

Watts, A. B., Tozer, B., Daly, M. C., & Smith, J. (2018). A comparative study of the Parnaíba, Michigan and Congo cratonic basins. In M. C. Daly, R. A. Fuck, J. Julià, D. I. M. MacDonald, & A. B. Watts (Eds.), *Cratonic Basin formation: A case study of the Parnaíba Basin of Brazil* (Vol. *472*, –66). Geological Society, Special Publications. https://doi.org/10.1144/SP472.6

Wittman, H., von Blanckenburg, F., Maurice, L., Guyot, J.-L., Filizola, N., & Kubik, P. W. (2011). Sediment production and delivery in the Amazon River basin quantified by in situ–produced cosmogenic nuclides and recent river loads. *GSA Bulletin*, *123*(5/6), 934–950. https://doi.org/10.1130/B30317.1

Zuffa, G. G. (1985). Optical analyses of arenites: Influence of methodology on compositional results. In G. G. Zuffa (Ed.), *Provenance of arenites* (pp. 165–189). NATO-ASI.

SUPPORTING INFORMATION

Additional supporting information can be found online in the Supporting Information section at the end of this article.

How to cite this article: Fellin, M. G., Zattin, M., Zuffa, G. G., De Ros, L. F., Cupertino, J. A., De Souza, R. S., Neto, J. M. M., & Dalmonte, C. (2023). New detrital petrographic and thermochronologic constraints on the Late Cretaceous–Neogene erosional history of the equatorial margin of Brazil: Implications for the surface evolution of a complex rift margin. *Basin Research*, *00*, 1–27. https://doi.org/10.1111/bre.12808